Iowa State University
Digital Repository

Retrospective Theses and Dissertations

Iowa State University Capstones, Theses and Dissertations

2008

Characterization of conductive surface printing via electric field induced ion transport

Khiam-How Low
Iowa State University

Follow this and additional works at: https://lib.dr.iastate.edu/rtd

Part of the Mechanical Engineering Commons

Recommended Citation
Low, Khiam-How, "Characterization of conductive surface printing via electric field induced ion transport" (2008). *Retrospective Theses and Dissertations*. 15458.
https://lib.dr.iastate.edu/rtd/15458

This Thesis is brought to you for free and open access by the Iowa State University Capstones, Theses and Dissertations at Iowa State University Digital Repository. It has been accepted for inclusion in Retrospective Theses and Dissertations by an authorized administrator of Iowa State University Digital Repository. For more information, please contact digirep@iastate.edu.

Characterization of conductive surface printing via electric field induced ion transport

by

Khiam-How Low

A thesis submitted to the graduate faculty

in partial fulfillment of the requirements for the degree of

MASTER OF SCIENCE

Major: Engineering Mechanics

Program of Study Committee:
Ashraf Bastawros, Major Professor
Abhijit Chandra
Thomas Rudolphi

Iowa State University

Ames, Iowa

2008

Copyright © Khiam-How Low, 2008. All rights reserved.

UMI Number: 1454643

INFORMATION TO USERS

The quality of this reproduction is dependent upon the quality of the copy submitted. Broken or indistinct print, colored or poor quality illustrations and photographs, print bleed-through, substandard margins, and improper alignment can adversely affect reproduction.

In the unlikely event that the author did not send a complete manuscript and there are missing pages, these will be noted. Also, if unauthorized copyright material had to be removed, a note will indicate the deletion.

UMI®

UMI Microform 1454643
Copyright 2008 by ProQuest LLC
All rights reserved. This microform edition is protected against unauthorized copying under Title 17, United States Code.

ProQuest LLC
789 East Eisenhower Parkway
P.O. Box 1346
Ann Arbor, MI 48106-1346

TABLE OF CONTENTS

ABSTRACT ...... **iv**

CHAPTER 1. INTRODUCTION **1**

1.1 BACKGROUND 1

1.2 FUNDAMENTAL CONCEPTS 2

1.3 PRINTING PROCESS DESCRIPTIONS 8

1.3.1 Method 1: Direct Contact Mask-Modulated Electric Field Printing 8

1.3.2 Method 2: Non-contact Mask-Modulated Electric Field Printing 9

1.3.3 Method 3: Non-contact Uniform Electric Field Mask Printing 12

1.4 AN OVERVIEW ON MATERIAL REMOVAL RATES (h^0) AND ASPECT RATIO (W/W_{mask}) 13

1.5 RESULTS COMPARISON OF THREE PRINTING METHODS 15

1.6 LITERATURE REVIEW 16

CHAPTER 2. EXPERIMENTAL PROCEDURE **23**

2.1 WORK PIECE PREPARATION 23

2.2 CHEMICAL SOLUTION (ELECTROLYTE) PREPARATION 25

2.2.1 Substance Measurements (Example calculations) 25

2.2.2 Making Chemical Solution Procedures 26

2.3 DIFFERENT TYPE OF MASKS (ELECTRODE) 28

2.4 EQUIPMENT AND EXPERIMENTAL PROCEDURE 30

2.4.2 Procedures 31

2.5 IMAGING ANALYSIS PROCEDURE 35

CHAPTER 3: EXPERIMENTAL RESULTS & DISCUSSIONS **36**

3.1 DIRECT CONTACT MASK-MODULATED ELECTRIC FILED PRINTING 36

3.1.1 TEM mesh with 80μm window opening 36

3.1.1.1 Imprinting under voltage control (CDC) 37
3.2 NON-CONTACT MASK MODULATED ELECTRIC FIELD PRINTING 41
3.2.1 Wire Mesh 41
3.2.1.1 Imprinting under current control (DC) 43
3.2.2 Perforated Stainless Steel 44
3.2.2.1 Imprinting under current control (DC) 45
3.2.2.2 Imprinting under current control (CDC) 46
3.2.2.3 Electrolyte Concentration Variation 50
3.2.2.4 Roll of the Cathode position 52
3.2.3 Polymer mask with a single 2.2 mm hole 56
3.2.3.1 Roll of applied pressure 56
3.2.3.2 Roll of standoff distance 59
3.2.4 TEM Mesh with 35µm Window Opening 60
3.2.4.1 Roll of applied pressure 60
3.2.4.2 Mesh insulation 62
3.2.4.3 Imprinting under voltage control (CDC) 63
3.3 NON-CONTACT UNIFORM ELECTRIC FIELD MASK PRINTING 65
3.3.1 TEM mesh with 35µm Window Opening 65
3.3.1.1 Imprinting under voltage control (DC) 65
3.3.1.2 Role of standoff distance 67

CHAPTER 4: CONCLUSIONS 72

CHAPTER 5: FUTURE WORK 75

REFERENCES 76

ACKNOWLEDGEMENT 78

ABSTRACT

A novel methodology to imprint micron size features on copper surface has been adopted in this study. The process of printing is based on focused electric field induced ion transport across a cation selective Nafion® membrane. The imprinting technology itself is environmentally benign because electrolyte consists of Sulfuric Acid (H_2SO_4) and Cupric Sulfate ($CuSO_4$) are encapsulated by Nafion® membrane in a copper made cathode chamber and it is sealed and recycled. In addition, the imprinted surface does not come in contact with corrosive chemicals which minimize the post cleaning process.

Three different methods of printing were embraced here in this study. They are direct contact mask-modulated electric field printing, non-contact mask-modulated electric field printing and non-contact uniform electric field mask printing. Process parameters for each type of methods have been studied in order to understand the effect on material removal rates, dimensions of the printed patterns compare to original mask and limitations on the printing process. The identified process parameters are the applied voltage, separation distance between two electrodes, variation on suctioned pressure, electrolyte concentration and conductivity, and variation of total pulse duration for the chopped direct current. Different mask types were used as an electrode to induce ions transportation. This include a 50PPI copper wire mesh, perforated stainless steel with Ø=570μm hole, polymer sheet with single drilled 2mm hole, copper TEM mesh with 35μm and 80μm window opening. Experimental results have shown that direct contact printing promises the best printing accuracy and geometric conformity among three methods, followed by mask printing with uniform electric field, especially for features in the range of tens of microns. Results from mask printing with

chopped DC voltage needs further improvement for features in the micron range to overcome lateral diffusion at many interfaces of the process as well as the divergence of the electric field within the electrolyte, the D.I. water and the ion transporting membrane.

CHAPTER 1. INTRODUCTION

1.1 BACKGROUND

The machining of materials on micrometer and sub micrometer scales is considered to be a key future technology. Micro-manufacturing technology has become an important topic in the fabrication of micro parts and devices such as micro-scale batteries, micro-fluidic systems, micro-holes for fiber optics, micro-nozzles for high-temperature jets, micro-molds and deep X-ray lithography masks, optical lenses, and micro components for a range of consumer electronics such as compact disc players, airbags and inkjet printers among many others (Rajurkar et al., 2006).

In conventional micro machining technology, mechanical micromachining and electro-physical and chemical processes (ECP) are two commonly used methods to produce micron and submicron scale surface patterning. During the mechanical micromachining process, direct contact with the work piece is established with good geometric correlation between the tool path and the work piece. However, this method has proven to be suitable for low-K porous dielectrics but not suitable for hard and fragile materials. Moreover, this method induces significant level of residual stresses and posses additional limitations on dimensional tolerances and minimum gage requirements (Liu et al., 2004).

An Electro-physical and chemical process (ECP) provides distinct advantages over mechanical micromachining by not contacting the work piece during micron and submicron scale surface patterning. The ECP eliminates the elastic spring back trouble and the minimum gage requirement to sustain the cutting forces. Electro-discharge machining (EDM) and

electrochemical machining (ECM) are two methods of ECP which has been widely used in the industry. ECM provides outstanding performance for manufacturing complicated three dimensional (3D) parts like crankshafts or gearwheels from hard materials (Kock et al., 2003) and also provides low material waste as well as minimized tool wear. On the other hand, the finished surface comes in contact with corrosive chemicals which may accelerate corrosion and require post ECM cleaning for the finished surface (Wilson, 1971).

1.2 FUNDAMENTAL CONCEPTS

Electric field is a region in space where an electric charge is experiencing electric force acting on it. The electric force, $\boldsymbol{F}$ on the charge, q is defined as

$$\boldsymbol{F} = q\boldsymbol{E} \tag{1.1}$$

where $\boldsymbol{E}$ is defined as the electric field strength and can be determined by the magnitude and positions of the charges acting on particular a charge q . The unit for $\boldsymbol{E}$ is Newton/Coulomb, N C^{-1}. Based on the positive and negative chargers, the electric field will act in opposite directions. The electric field strength $\boldsymbol{E}$ at a distance r away from the point charge (Figure 1) is given by,

$$\boldsymbol{E} = \frac{q}{4\pi\varepsilon_0 r^2}\boldsymbol{u} \tag{1.2}$$

where $\boldsymbol{u}$ is a unit vector from the point charge, ε_0 is the vacuum permittivity which

$$\varepsilon_0 = 8.85418 \times 10^{-12} \mathrm{C^2\,N^{-1}\,m^{-2}}$$

Electric field lines can be described as joining force vectors of a vector map so that the field lines passing through any point are the tangent to the field vector at that point. Magnitudes of the force per unit charge exerted on any test charge placed at a point along a particular field line are not the same. The intensity of the field for an arbitrary point is characterized by the number of line passing through unit area about that point. This also means that high density of field lines has larger field intensity. The equipotential contour through any point must be perpendicular to the field line. When equipotential contours are closely spaced, the potential changes drastically over a short distance and the potential gradient is high; as potential contours spaced wider, the field intensity will become lower (Figure 1).

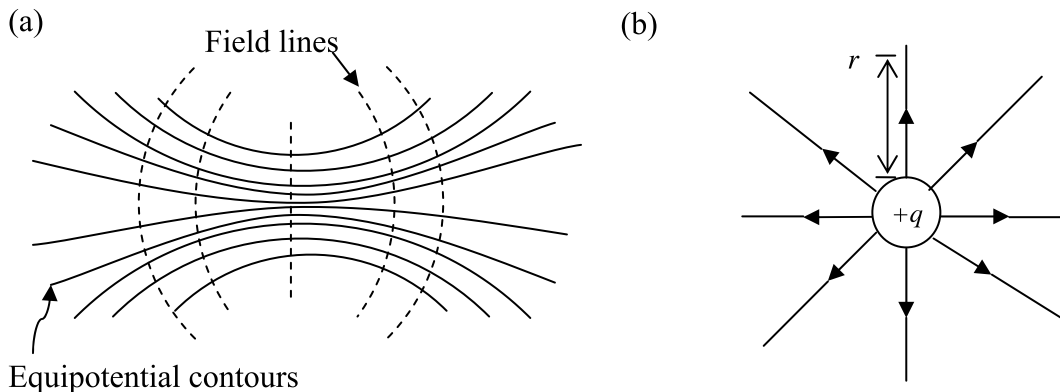

Figure 1 (a) Changes of field intensity as equipotential lines vary and (b) Field strength of a positive point charge *q*.

Electric field from a symmetric charge distribution surface can be calculated from Equation (1.2) by considering the charge distribution is accumulation of individual point

charges and adding the field strengths from these charges. It can also be calculated by applying Gauss' Law

$$\oint \boldsymbol{E} \cdot d\boldsymbol{S} = \frac{q}{\varepsilon_0}$$

(1.3)

which is taking surface integral over the any closed surface of the normal component of the electric fields equals the enclosed charge divided by the vacuum permittivity.

Work done to move a charge, q from point A to point B is being defined as

$$W_{AB} = q \int_A^B \boldsymbol{E} \cdot d\boldsymbol{x}$$

(1.4)

The potential difference between point A and B in a electric field is defined as

$$V_A - V_B = \int_A^B \boldsymbol{E} \cdot d\boldsymbol{x}$$

(1.5)

and the unit for potential difference is Joule/Coulomb (J C^{-1}) or most often as volt (V).

Concept of capacitance is introduced when a conductor is being insulated. Capacitance of a conductor determines the energy that is stored in the system for a given charge. The unit for capacitance is charge/voltage, coulomb/volt. It is commonly defined as farad, F as

$$1\ \text{F} = 1\ \text{C}\ \text{V}^{-1}$$

(1.6)

Parallel plate capacitor consists of two normally plane planes as shown in Figure 2. The negative terminal of the plate is being grounded and by induction, a charge of opposite polarity q will be bounded on that terminal. Charges are located at the sides of the plates

facing each other and the electric field is distributed homogeneously in the region between the plates, the area of the plate is defined as "A". Since charges do not exist outside the plate, the electric field will be zero in that region.

Similar to previous equation

$$\oint \boldsymbol{E} \cdot d\boldsymbol{S} = EA = \frac{q}{\varepsilon_0}$$

(1.7)

$$E = \frac{q}{A\varepsilon_0}$$

(1.8)

Potential difference between plates

$$V = Ed = \frac{q}{A\varepsilon_0} d$$

(1.9)

Capacitance is then defined as

$$C = \varepsilon_0 \frac{A}{d}$$

(1.10)

The above equation is used when the region between two plates is filled with air, gases or vacuum. If dielectric or insulator exists in between plates, a relative permittivity or dielectric constant, ε_r needs to be incorporated into equation yields

$$C = \varepsilon_0 \varepsilon_r \frac{A}{d}$$

(1.11)

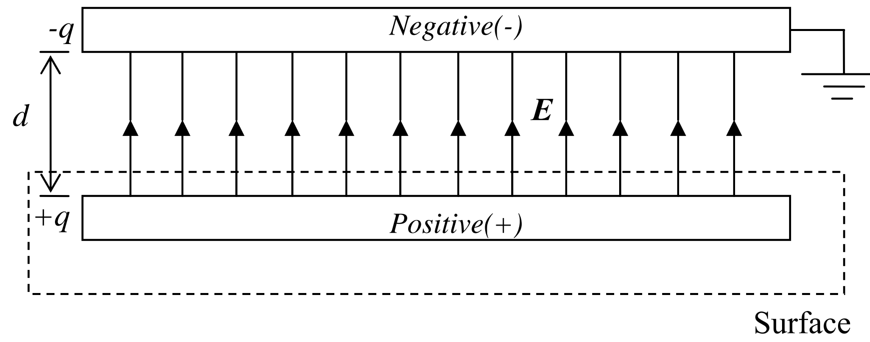

Figure 2 Parallel plate capacitor.

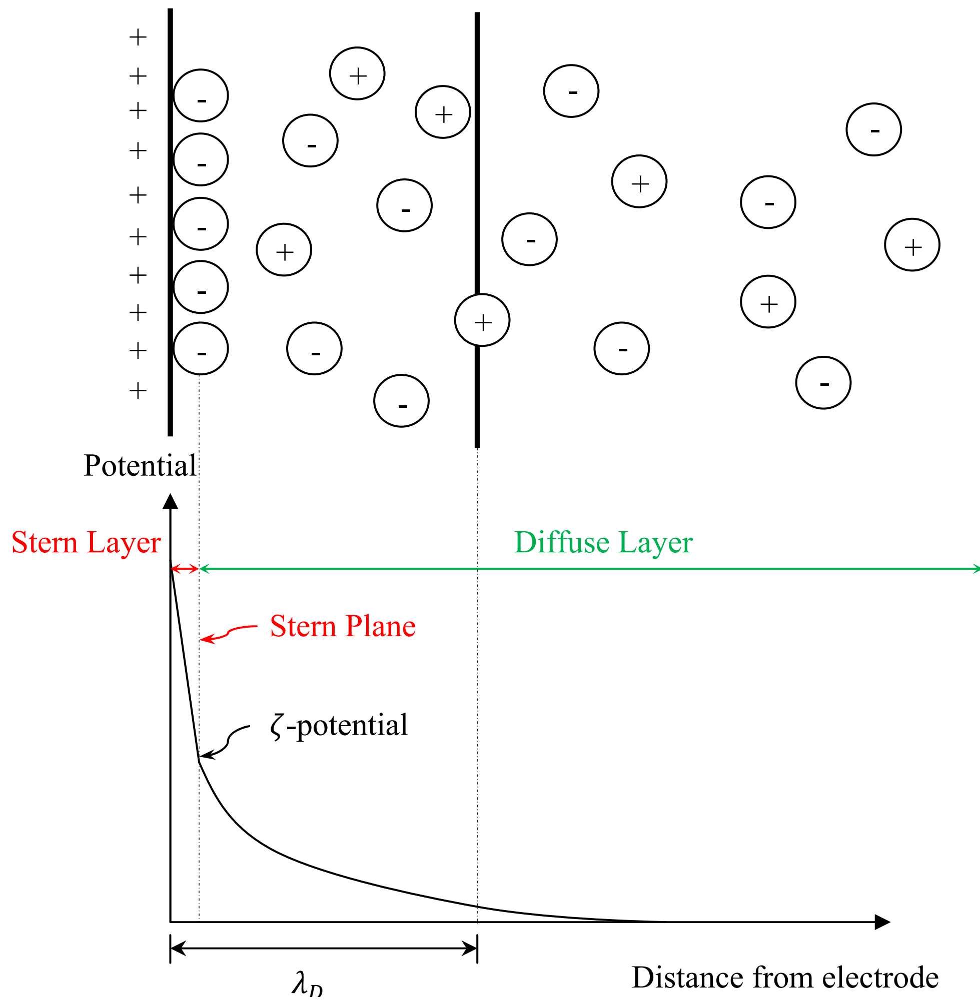

Figure 3 Structure of Electric Double Layer (EDL).

In the case where a charged surface is in contact with an electrolyte regardless of the strength of the electrolyte (weak or strong), the charged surface will attract the ions of the opposite charge in the electrolyte and form an electric double layer (EDL) or so called Debye layer as shown in Figure 3. The ions on the inner layer of the EDL are static and will not migrate due to any external field applied. However, the outer layer or so called the diffusive layer may be affected by an external electric field. The thickness of the EDL is characterized by the Debye length, λ_D which is found by balancing repulsive diffusive forces with attractive electrical forces. Debye length is defined as

$$\lambda_D = \frac{1}{\kappa} = \sqrt{\frac{\epsilon KT}{2e^2z^2c}}$$

(1.12)

κ is the aspect ratio, ϵ is the dielectric constant, C (V m)$^{-1}$, e is the elementary charge, 1.602×10^{-19}C, z is the number of charges and c is the Molar concentration mol m^{-3} of the bulk solution (Brask A., 2003). From Equation (1.12), thickness of the double layer depends on temperature, concentration and number of ions. As the temperature increases, bombardments of the ions are more frequent and lead to a reduction of the shielding layer. The shielding is more effective at higher concentration level because of the charge density is greater. Poisson’s equation is used to correlate electric field and charge density,

$$\nabla^2\emptyset = -\frac{\rho E}{\epsilon}$$

(1.13)

1.3 PRINTING PROCESS DESCRIPTIONS

Nafion® membrane is a type of perfluorosulfonic acid (PFSA) product which is categorized in the class of synthetic polymers with ionic properties called ionomers. Nafion membrane is adapted for this study because of its excellent conductive properties and it allows permeability of anions but provides an effective barrier for cation or electrons. In addition, Nafion® membrane acts as a separation barrier between the electrolyte and Deionized (D.I.) water which does not allow electrolyte to contaminate the work piece during the process.

1.3.1 Method 1: Direct Contact Mask-Modulated Electric Field Printing

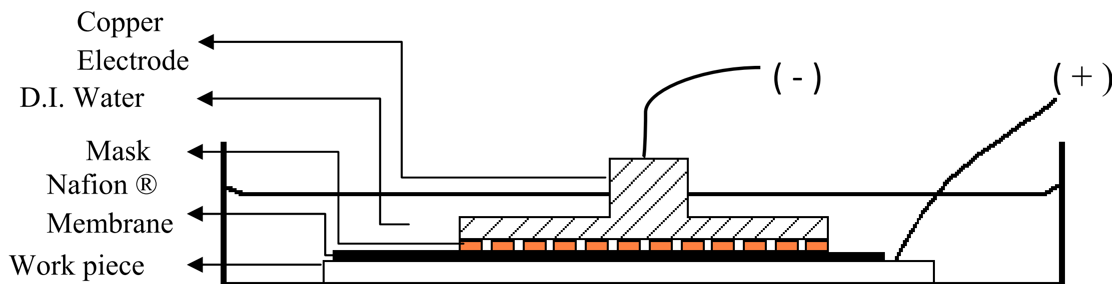

Figure 4 Experimental Configuration for direct contact printing method.

Similar process principle as investigated by Husser (1989) and Craston (1988), the experiment configuration for this method is shown in Figure 4. Nafion® membrane is directly in contact with work piece and mask/electrode is placed on top. Function of copper stud is used as conducting electricity to the mask as well as applying uniform pressure on the mask to prevent it from floating on the D.I. water. When surface contact is made between the bottom of mask and the surface of the Nafion® membrane, a faradaic current passes and

metal ions are being reduced to metal at the contacting interface. It is assumed that the applied potential is adequately large that the kinetics of the electrode are not rate limiting. The current obtained when the conductive mask makes contact with the Nafion® membrane will depend on the rate of mass transport of metal ions transfer to the bottom of the mask. The result is a reduction process at the mask and membrane interface (deposition) and an oxidation process at the work piece (etching).

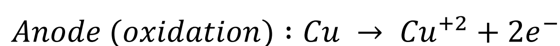

$$Anode\ (oxidation): Cu \rightarrow Cu^{+2} + 2e^-$$

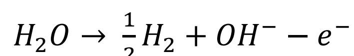

$$H_2O \rightarrow \frac{1}{2}H_2 + OH^- - e^-$$

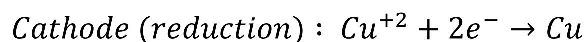

$$Cathode\ (reduction):\ Cu^{+2} + 2e^- \rightarrow Cu$$

1.3.2 Method 2: Non-contact Mask-Modulated Electric Field Printing

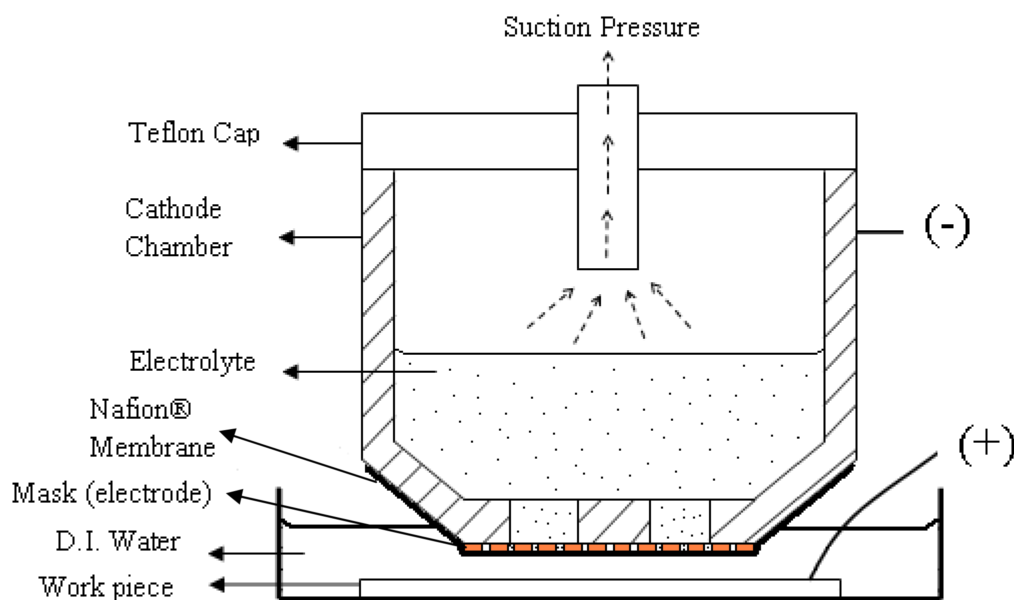

Figure 5 The processing cell for mask-modulated electric field printing. Nafion membrane is adhered to the mask and preventing electrolyte inside the cathode chamber contaminating D.I. water. Thus, make it chemical free on copper work piece surface.

The processing cell for this method is shown in Figure 5. The processing cell consists of a copper made cathode chamber which is cavity filled with electrolyte, a mask with window openings as an electrode attached to the bottom of the chamber where Nafion® membrane adhered to it, a copper work piece as anode and immersed under the D.I. water. Aqueous sulfuric acid and cupric sulfate are used as electrolyte in this study. During the process when a potential difference is applied, current flows between two terminals and the metal ions flow towards the charge-selective membrane to be deposited over the cathode chamber. For example, the copper ion is oxidized at the anode from zero valence state to form cations with a positive charge by losing two electrons; at the cathode terminal, copper ion is reduced to copper particle by gaining two electrons.

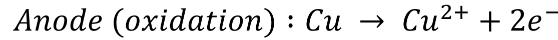

$$Anode\ (oxidation) : Cu \rightarrow Cu^{2+} + 2e^-$$

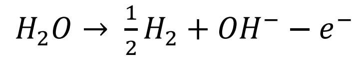

$$H_2O \rightarrow \frac{1}{2}H_2 + OH^- - e^-$$

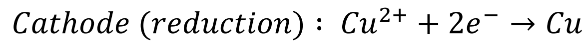

$$Cathode\ (reduction) : Cu^{2+} + 2e^- \rightarrow Cu$$

Migration of Cu^{+2} from anode to cathode through the Nafion® membrane does not contaminate the D.I. water thus the process is environmental friendly.

Ions migration is limited to the window opening of the mask (electrode) as they transfer across the boundary of Nafion® membrane. The local material removal is defined as

$$\boldsymbol{J}(\boldsymbol{x}) = -D\boldsymbol{\nabla}\boldsymbol{C}(\boldsymbol{x}) - \frac{nFDC_0\boldsymbol{\nabla}\emptyset(\boldsymbol{x})}{RT}$$

$$= -D\boldsymbol{\nabla}\boldsymbol{C}(\boldsymbol{x}) - \frac{\kappa\boldsymbol{\nabla}\emptyset(\boldsymbol{x})}{nFR_e}$$

(1.14)

where D is the diffusion coefficient

$\boldsymbol{C}(\boldsymbol{x})$ is the ion concentration at the interface with the boundary layer

C_0 is the average ion concentration in the solution bulk

$\emptyset(\boldsymbol{x})$ is the local electric potential wherein the electric field $\boldsymbol{E}(\boldsymbol{x}) = \boldsymbol{\nabla}\emptyset(\boldsymbol{x})$

n is the number of electrons transferred in the oxidation reaction

F is the Faradic constant, $96485\ C\ mol^{-1}$

R is the universal gas constant

T is the absolute temperature

R_e is the electrolyte resistivity

The local material removal rate can be determined as

$$\dot{\boldsymbol{H}}(\boldsymbol{x}) = \frac{\boldsymbol{J}(\boldsymbol{x})M}{\rho}$$

(1.15)

Where M is the atomic weight ($M_{copper} = 63.546\frac{g}{mol}$)

ρ is the density of the anode material ($\rho_{copper} = 8.96\ \frac{g}{cm^3}$)

By varying the pressure applied inside the cathode chamber relative to ambient pressure, local curvature on the membrane can be achieved. The local curvature of the membrane will modulate the equipotential electric field to focus the electric current on the

work piece and a pattern with aspect ratio smaller than the original window mask size can be achieved. Besides pressure variation, the depth and aspect ratio on the pattern are controlled by process parameters such as separation distance between two terminal, amount of potential energy that applied (voltage), total exposure time as well as concentration of the electrolyte used. A well defined mask (electrode) with precise window opening is mandatory to achieved pattern in micron range.

1.3.3 Method 3: Non-contact Uniform Electric Field Mask Printing

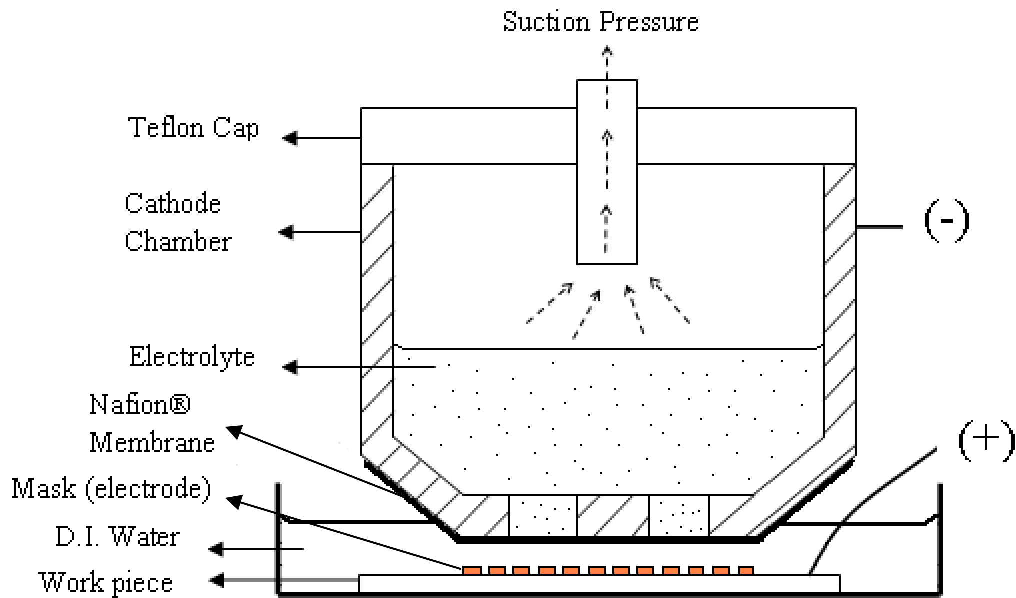

Figure 6 The processing cell for uniform electric field mask printing. Notice that the configurations are identical to the printing method 2 except the mask/electrode is placed on the surface of the work piece.

The experiment configuration of this mask printing under uniform electric field consist of a copper cathode chamber, work piece, Nafion® membrane, mask and D.I. water. The difference between the previous method and uniform electric field method is by locating

the mask on the work piece. Migrations of Cu^{2+} ions are only limited at the mask opening area and a well defined etching pattern on the work piece can be achieved. Similar to the altering electric field method, the mass transfer from the electrode under steady state conditions is governed by Nernst-Planck equation.

1.4 AN OVERVIEW ON MATERIAL REMOVAL RATES (h^0) AND ASPECT RATIO (W/W_{mask})

(a)

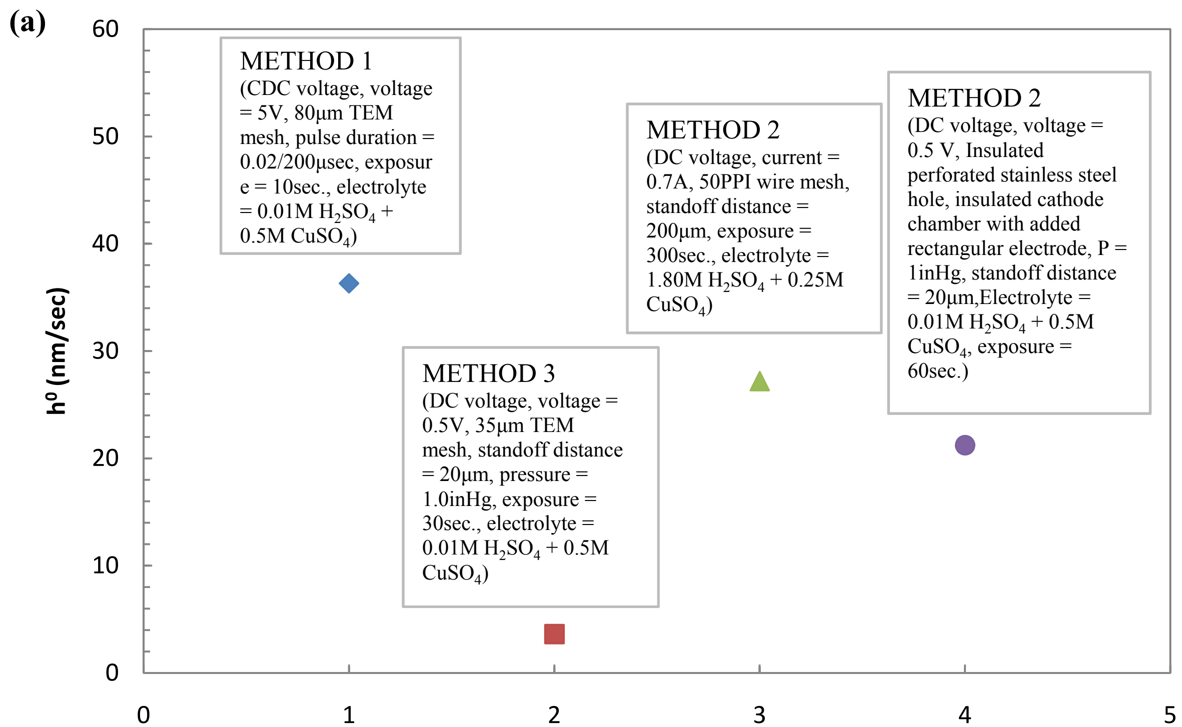

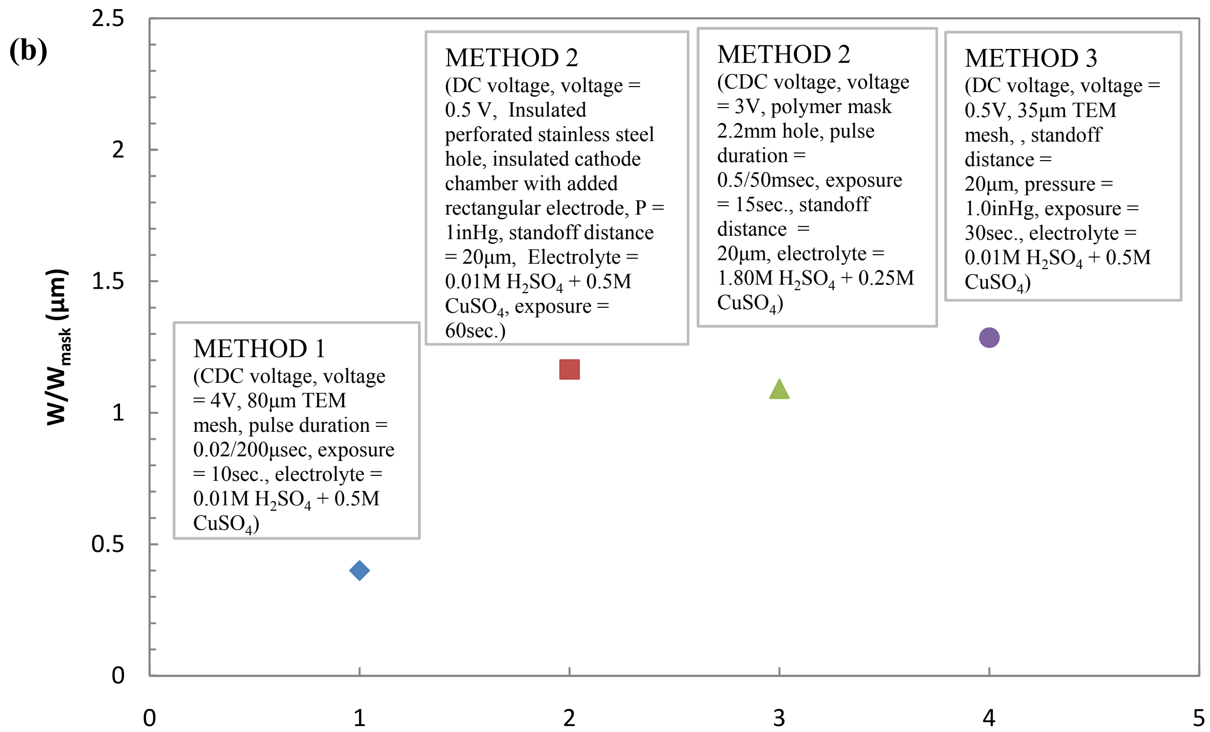

Figure 7 Comparison on (a) material removal rates (h^0) and (b) aspect ratio (W/W_{mask}) for different printing methods as well as process parameters. METHOD 1: Direct Contact Mask-Modulated Electric Field Printing, METHOD 2: Non-contact Mask-Modulated Electric Field Printing, METHOD 3: Non-contact Uniform Electric Field Mask Printing.

Material removal rates and the aspect ratio (Figure 7(a) (b)) were investigated with correlations on studying different process parameters as discussed earlier in abstract. The process parameters are applied voltage, separation distance between two electrodes, variation on suctioned pressure, electrolyte concentration and conductivity, and variation of total pulse duration for the chopped direct current. Figure 7(a) and (b) are to provide an insight on three printing methods as well as utilizing different mask types have successfully achieved reasonable h^0 and W/W_{mask}.

1.5 RESULTS COMPARISON OF THREE PRINTING METHODS

A representative printing pattern for each of the three printing configurations is shown in Figure 8 to elucidate the characteristics and performance of each configuration. The best resolved pattern is typically acquired from the direct printing method.

(a) Method 1: Direct Contact Mask-Modulated Electric Field Printing (Mag.=10X)

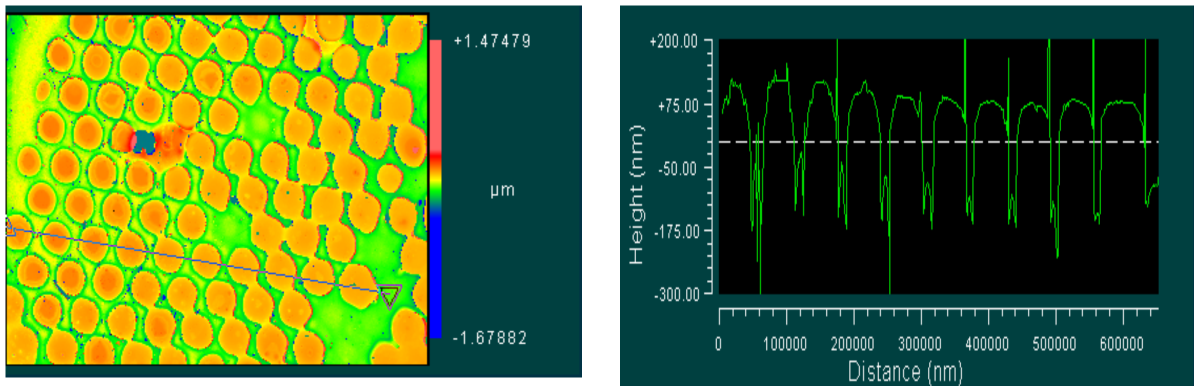

(b) Method 2: Non-contact Mask-Modulated Electric Field Printing (Mag.=10X)

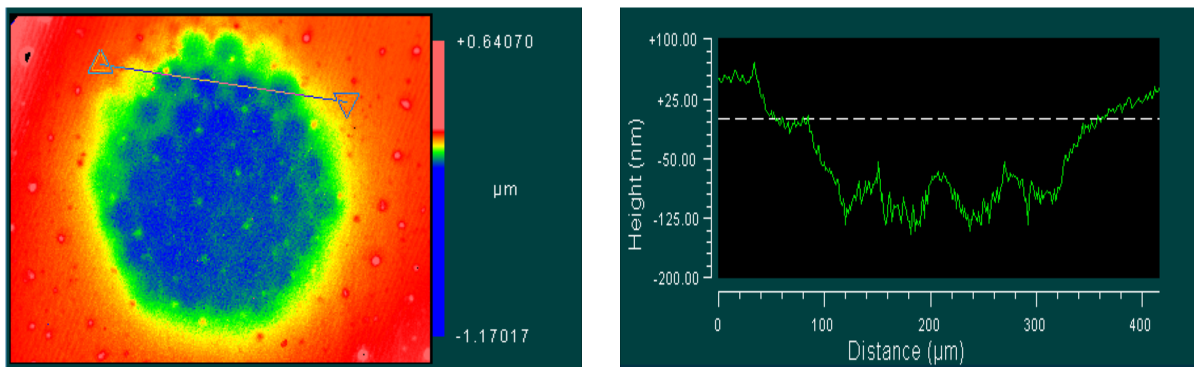

(c) Method 3: Non-contact Uniform Electric Field Mask Printing (Mag.=10X)

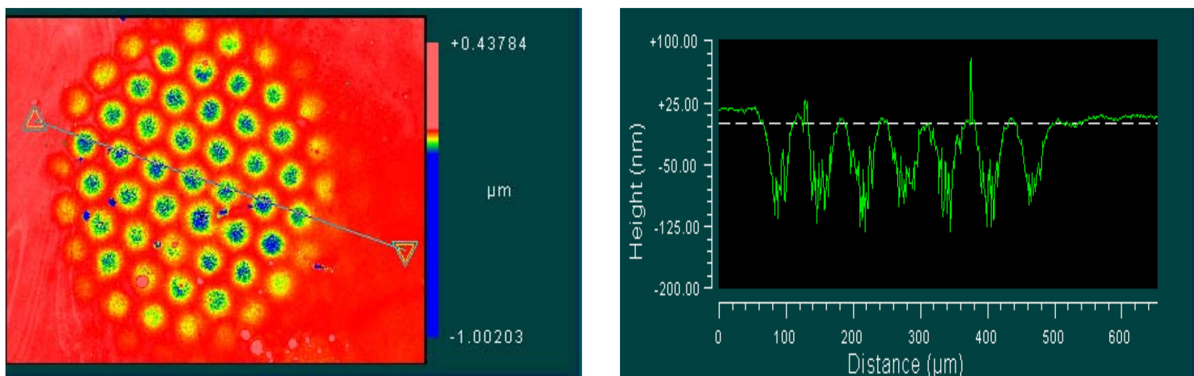

Figure 8 Results comparison of three different printing methods. (a) Direct contact printing under CDC voltage (5V, pulse duration = 0.02/200μsec., exposure= 10sec. (b) Mask printing under DC voltage (0.1V, standoff distance = 20μm, P= 1.0inHg, exposure= 30sec., electrolyte = 0.01M H_2SO_4 + 0.5M $CuSO_4$. (c) Mask printing under uniform DC voltage (0.1V, standoff distance = 20μm, P=1.0inHg, exposure = 30sec., electrolyte = 0.01M H_2SO_4 + 0.5M $CuSO_4$).

1.6 LITERATURE REVIEW

This section summarizes some of the relevant previous work related to electrochemical machining (ECM) as well as electrochemical polishing and closely related field.

A method by which electrochemical reactions on conducting materials can be localized with sub micrometer precision was examined by Schuster et al. (2000) and Kirchner et al. (2001). They achieved sub micrometer precision by applying very short voltage pulses of only nanosecond duration. Their method was different than conventional ECM in which the applied DC-voltage causes the uniform dual layer (DL) charging and the reaction rate was mainly defined by the current density in the electrolyte. The conventional method could only provide limited spatial resolution of roughly 100μm. Their concept can be illustrated by a simplified equivalent circuit of two electrodes immersed in electrolyte. The charging current has to flow through the electrolyte whose resistance is proportional to length of separation between two electrodes. A locally varying time constants was defined $\tau = \rho d c_{dl}$ for the charging of the dual layer which depending on the separation d between the electrodes, the specific electrolyte resistivity ρ and the specific dual layer capacity c_{dl}. When the pulse time is bounded by the defined time constant τ, the electrode surface would be charged. As a

result, the polarization effect of the dual layer will reach appreciable values only near the very tip of the tool electrode. Thus, the electrochemical processes will be confined to electrode regions in close proximity to the electrode.

Similar electrochemical micromachining with ultra short voltage was performed by Kock et al. (2003). The results show the role of further reducing the pulse duration from 5 μs to 100 ns on accuracy improvement of the machined profile (Figure 9). For a given separation distance of 1μm between the electrode and the work piece, the gap clearance around the electrode increases linearly with the pulse duration. Once the gap clearance becomes comparable to the tool electrode dimension, the gap would modestly increase with the increase of pulse duration (Figure 10). At this instant, the active surface area of the tool where the dual layer is polarized during the pulse voltage becomes smaller than the workpiece. Consequently, the DL capacitance would drop, deteriorating the amplitude of the applied pulse. As the gap clearance went larger than the tool electrode diameter, the dual layer on the workpiece became less polarized than the tool dual layer and therefore decreased the dissolution rate of the material.

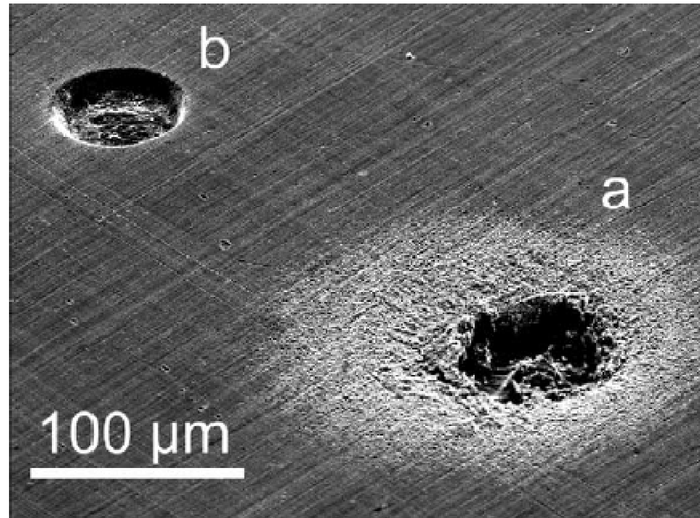

Figure 9 Two holes etched into a Cu sheet, employing a cylindrical Ø 50 um Pt tool. (a) Applying 5 µs pulse duration. (b) Pulse duration reduced to 100 ns which significantly improved the precision of electrochemical machining.

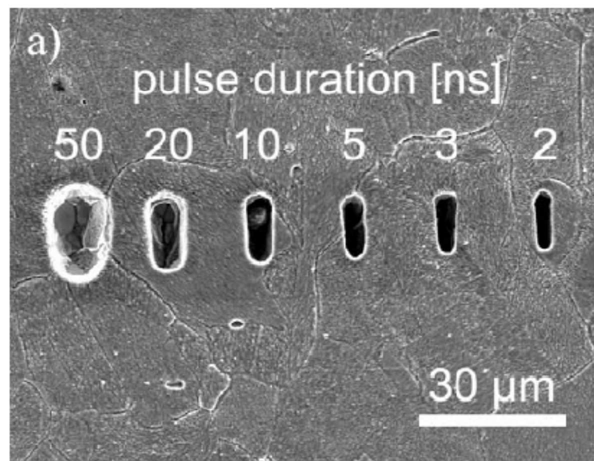

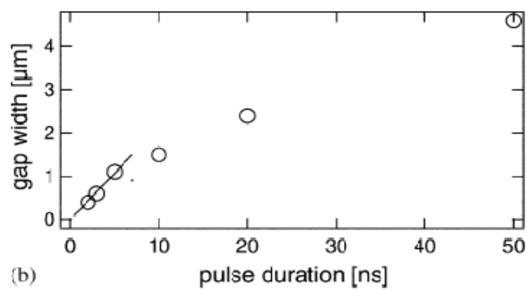

Figure 10 (a) Troughs etched into Ni with various pulse durations. (b) Spatial resolution, the width of the lateral gap between the tool electrode and the workpiece obtained for different pulse duarations.

The work of Lee, Baek and Cho (2004) showed that microholes with size of 50 µm in diameter could be accurately machined as well as further improvement of the surface roughness could be achieved when pulse electric current was applied. Their results showed that the material removal (machining depth) increased with the pulse time, T_{on}, for a fixed duty factor ($T_{on}/(T_{on}+T_{off})$). The hole diameter was also increased by increasing the voltage, for a fixed T_{on}. The material removal rate was much faster at the initial stage and continued with a slower rate after fifteenth seconds of the machining time (Figure 11).

(a)

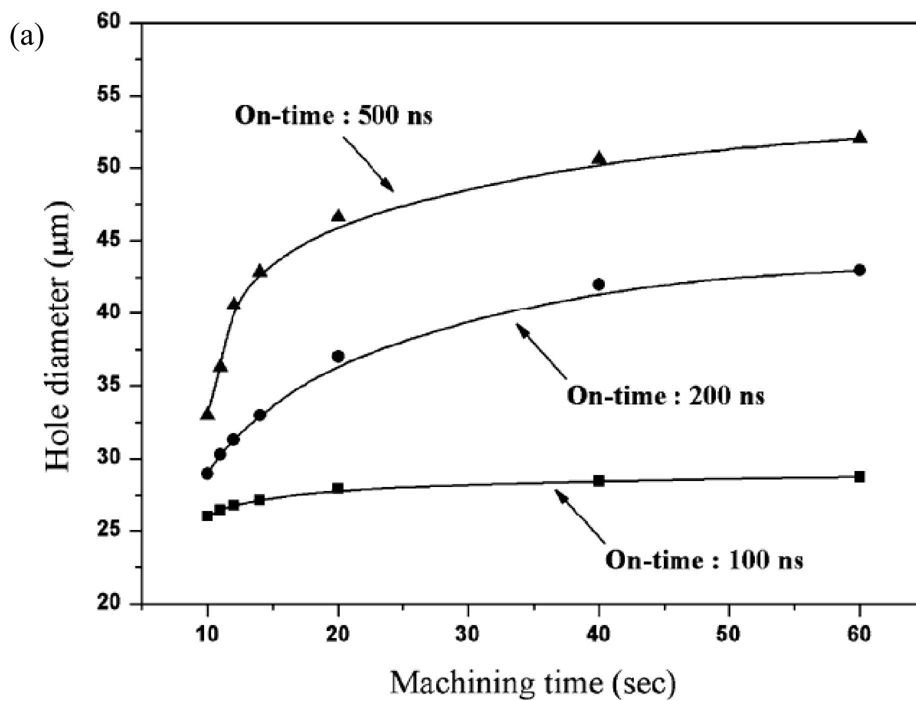

(b)

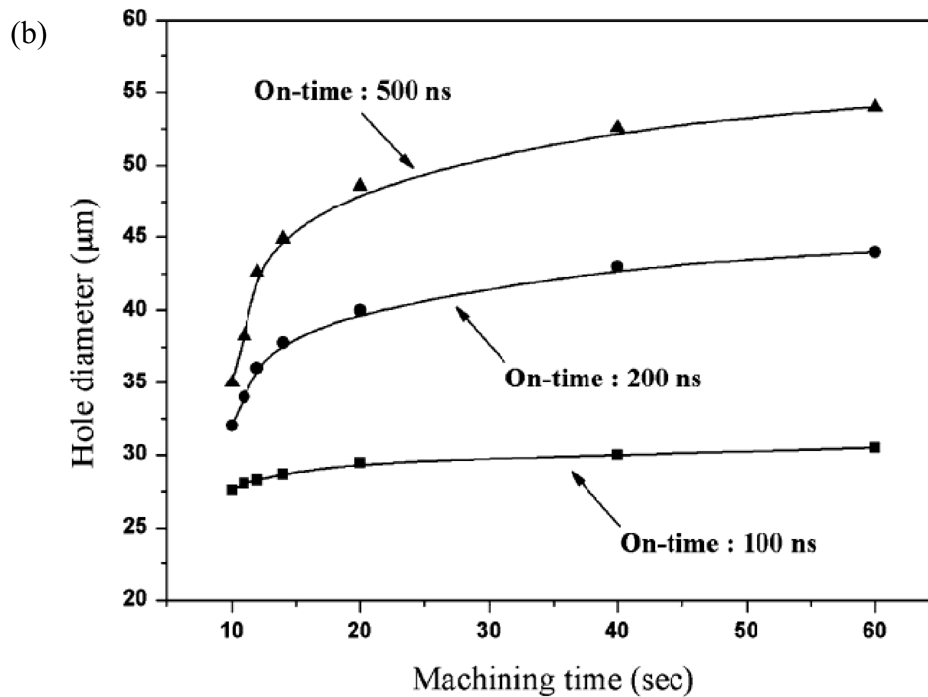

Figure 11 Comparison on the hole diameter by applying (a) 1.5 V, (b) 2 V with pulse duration fixed at 1-μs.

Membrane-mediated electropolishing (MMEP) is a new process used for planarizing and polishing a metal anode using a charge-selective ion-conducting membrane to separate the cathode and electrolyte solution from the work piece through a thin layer of deionized water covering the workpiece surface. Mazur et al. (2007) in their experimental study on MMEP of copper showed that by controlling the process parameters, a planarization and removal of excess copper process could be done more efficiently than the conventional chemical-mechanical polishing (CMP) process. The process parameters include the interfacial velocity of the rotating work piece, the current density of the process and concentration of the electrolyte solution. Their results on static etching (without rotating the work piece) showed that as they increased the amount of charges in the system, the majority of the material was removed from a thin trench around the edge of each island while less

material was removed from the area facing the channel on the membrane. The 2D profile of the etched pattern could be depicted as a “Vampire’s teeth”. Their explanation regarding this phenomenon was due to inadequate water content to maintain the conductivity of membrane in the area facing the channel while diffusion from the surrounding bulk liquid can maintain an adequate flux of water to compensate for the electro-osmosis loss.

Scanning electrochemical microscope is a modified version of scanning tunneling microscope (STM). A study on using scanning electrochemical microscope (SECM) to deposit and etch materials was investigated (Husser et al. (1989), Craston et al. (1988)). The experimental result has proven that the SECM method could achieve a resolution in the submicron range. The fundamental experimental concept is bringing the tip of the SECM which acted as cathode terminal in contact with the work piece surface. A thin layer of ionically conducting polymer which contains mobile ions is used to separate the tip from the work piece surface. By applying certain potential, the faradaic current results in a reduction process at the tip on the polymer interface and an oxidation reduction at the work piece substrate surface. Thus, localized etching on the work piece surface can be achieved by moving the tip electrode. They did mention in their findings that a very low amount of current in the range of nano-Ampere (nA) was applied. However, the area of the SECM tip was not mentioned in their findings and current density was not able to calculate.

Investigations on water uptake and transport through ionomeric fuel cell membranes were studied by Zawodski et al. (1993). In their studies, they experimentally investigated the diffusion coefficient and conductivity on the perfluorosulfonic acid membrane from different manufacturer. They found that the thickness of the membrane was an important parameter in

determining the efficiency of the membrane due to aforementioned competition between electro-osmotic drag as well as the back-diffusive fluxes in determining membrane water profiles. For higher density of the ionic groups combined with higher water content per sulfonic acid, the protonic conductivity yielded a much larger value. Higher temperature yielded a lower conductivity of the membrane due to rehydration of the membrane and all water was lost from the membrane.

Solasi, Zou and Huang (2007) have shown that Nafion membrane exhibits strong time and rate effect dependency on temperature and hydration. They were performing experimental work (uniaxial tension test) as well as doing finite element modeling to find stress-strain characteristic of Nafion membrane at different strain rates with respect to different temperature and hydration settings. Nafion membrane dependency on temperature and hydration were due to phase inversion and cluster formation.

Test Condition	Elastic		Plastic	
	E_e (MPa)	ν	$\sigma_1$at $\varepsilon_p =$ 0(MPa)	$\sigma_1$at $\varepsilon_p =$ 1(MPa)
$T = 26$ °C & RH = 50%	150	0.4	3.5	18.2
$T = 26$ °C & RH = 3% (Dry)	225	0.4	1.4	32.5
$T = 26$ °C & RH = 87% (Humid)	100	0.4	0.8	23

Table 1 Elastic-plastic parameters.

CHAPTER 2. EXPERIMENTAL PROCEDURE

Details of the experimental procedures including preparation of imprinted surface, experimental setup for the printing process as well as pattern analysis are given in this chapter.

2.1 WORK PIECE PREPARATION

Two types of imprinted surfaces were used in the current study; (i) high purity, oxygen free copper discs, and (ii) an e-beam sputtered copper layer of 100-500nm on glass slides. Copper disc was used particularly for larger windows opening mask type like 50PPI copper wire mesh, Ø=570 μm perforated stainless steel, polycarbonate mask with five Ø=380 μm vias, polymer mask with a single Ø=2 mm hole. E-beam spattered copper films were used for smaller windows opening mask type, particularly TEM mesh with 80 μm and 30 μm windows opening and finer features of several microns.

All copper discs were ground then polished with alumina slurry. The final polishing process was in a chemically active slurry as a chemical mechanical polishing (CMP) to achieve about 10-20nm surface roughness over several hundreds of microns. Chemical Mechanical Polishing is a surface planarization process used in microelectronics industry which employs the combined action of chemical dissolution and mechanical abrasions. Beuhler® Ecomet 4 variable speed grinder-polisher was used to perform the polishing process. The following procedures would be a guideline for achieving high surface quality. Depends on the surface roughness, copper disc was polished starting with Buehler™ 400 grit grinding paper, then to 600 grit grinding paper, 1 μm polishing pad with alumina slurry and

finally to 0.05 μm polishing pad with alumina slurry. Copper discs were mounted on the aluminum struts by melting catalyst on the Corning® hot plate. Three or six copper discs were loaded on Beuhler® specimen holder for polishing. 400 grit and 600 grit grinding paper were first used to planarize a reference surface. During this stage, the polishing process parameters were chosen as: down force of 1 to 2 lb., rotational speed of 70-80 rpm, identical rotational direction for wafer and grinding paper, polishing time of three minutes for one cycle. Two cycles for 400 grit and three cycles for 600grit were found to be most efficient for polishing a batch of newly manufactured copper discs. More cycles were spent on removing major scratches and surface peaks in this polishing stage before starting the 1 μm polishing stage. Beuhler® suspension α-alumina with particle size of 1 μm and Microcloth pad were used to further improve the surface quality. The surface polishing process was finished at Beuhler® suspension α-alumina with particle size of 0.05 μm. The polishing process parameters for particle size 1 μm and 0.05 μm: down force of 1 lb., rotational speed of 80 rpm, identical rotational direction for wafer and pad, polishing time of three minutes for one cycle. All polished copper discs were rinsed by tap water to remove excessive polishing suspension and blow-dry by using an air gun.

The heating process was repeated in order to remove copper disc from the aluminum struts. Acetone was used to remove excessive catalyst on the back of the copper disc and rinsed by using distilled water. All copper discs were blown to dry by air gun and kept in an air tight container.

2.2 CHEMICAL SOLUTION (ELECTROLYTE) PREPARATION

In order to allow cation to transfer to the wall of cathode chamber (negative terminal), electrolyte as a bridge was meant to fulfill the task. Cupric Sulfate ($CuSO_4 \cdot 5H_2O$) [Fisher Scientific C493-500], Sulfuric Acid (H_2SO_4) [Fisher Scientific A298-212] and deionized water are three major components in making electrolytes for this study. Electrolyte used in this study was prepared carefully with the calculated correct amount of substance need to be added to yield the targeted conductivity (S/cm) or PH. Example calculations on finding correct quantity of chemicals need to be added as well as details procedures in making electrolytes are given below as a guideline.

2.2.1 Substance Measurements (Example calculations)

Element	Atomic weight
Copper	63.546
Sulfur	32.066
Oxygen	15.9994
Hydrogen	1.00794

Table 2 Atomic weight of elements.

In order to make $\mathbf{0.25\,mol/L\ CuSO_4 + 1.80\,mol/L\ of\ H_2SO_4}$ **+ D.I. water**:

$$CuSO_4 : 63.55 + 32.07 + (15.9994 * 4) = 159.608 \frac{g}{mol}$$

$$5H_2O : 5 * \{(1.007 * 2) + 15.999\} = 90.065 \frac{g}{mol}$$

$CuSO_4 \cdot 5H_2O : [159.608 + 90.065] = 249.673 \frac{g}{mol}$

$H_2SO_4 : (1.007 * 2) + 32.066 + (15.999 * 4) = 98.076 \frac{g}{mol}$

To find Cupric Sulfate in terms of $\frac{g}{L}$

$$0.25\frac{mol}{L}\ of\ CuSO_4 \cdot 5H_2O\ :\ 249.673\frac{g}{mol} * 0.25\frac{mol}{L} = 62.4183\frac{g}{L}$$

To find Sulfuric Acid in terms of $\frac{g}{L}$

$$1.80\frac{mol}{L} of\ H_2SO_4 : 98.076\frac{g}{mol} * 1.80\frac{mol}{L} = 176.537\frac{g}{L}$$

If we are making $\mathbf{650\ mL}$ of solution,

$CuSO_4 \cdot 5H_2O$ in 0.65 L : $62.4183\frac{g}{L}$ * 0.65 L : 40.5719 g

H_2SO_4 in 0.65 L : $176.537\frac{g}{L}$ * 0.65 L : 114.749 g

40.572 g of Cupric Sulfate and 114.749 g of Sulfuric Acid are to be prepared and mixed in the electrolyte.

2.2.2 Making Chemical Solution Procedures

For mixing the solution, the following were utilized: beakers, stainless steel spatula, Corning® hot plate with magnetic stir bid, deionized water (D.I. water), Copper (II) Sulfate ($CuSO_4$), Hydrochloric Acid (H_2SO_4). Chemical apron (heavy latex) and goggles were always worn as safety precautions for making chemical solutions procedures. All chemical solutions substances and liquids needed for mixing purposes were gathered under the fume hood. Apparatus such as beakers and stainless steel spatula were washed twice by using filtered tap water to prevent residues from contaminating the electrolytes.

Weighing balance was moved under the fume hood in order to measure amount of substance needed and also to ensure all chemicals were supposed to handle under the hood. Beaker was placed on the balance and zeroed. Calculated amount of $CuSO_4$ in terms of gram (g) was then added into the beaker by using cleaned spatula. Desirable amount of Deionized water (D.I. water) was added to the beaker just to dissolve the $CuSO_4$ before

adding H_2SO_4. Beaker with substance was moved to a Corning® hot plate with magnetic stirrer.

A cleaned beaker was placed on the weighing machine in order to measure the correct amount of Hydrochloric Acid. Previous step was repeated in order to zero the weight for the beaker. Pipette was used to transfer adequate amount of H_2SO_4 into the beaker from acid bottle. The amount of acid needed was measured and be sure the acid bottle cap was shut properly and being placed back to the original location. Acid in the beaker was slowly poured into the beaker containing $CuSO_4$ and D.I. water and started with stirring. It was also an important step that sufficient amount of stirring was required to release the heat generated due to chemical reaction between H^+ and OH^-. Be sure that strong acid like Hydrochloric Acid had to be added slowly to the beaker containing D.I. water but not the inverse of the step. Adding large amount of H_2SO_4 suddenly into the D.I. water would lead to huge amount of heat generation and sudden splashing of chemical solution would contact the person nearby. Immediate assistance would be required if large amount of chemical solution contacted to the person eyes or body.

Approximately fifteenth to twenty minutes of time would be required to completely dissolve all the $CuSO_4$ in the solution. Additional time would be required to dissolve all $CuSO_4$ depends on the quantity of the salt. PH meter and Conductivity meter were used to measure the acidity and conductivity of the solution before saving it into a clean glass bottle.

2.3 DIFFERENT TYPE OF MASKS (ELECTRODE)

Different types of mask were used to create specific pattern on the work piece surface as well as to study the limitation on the achieved resolution. Experimentally, the purpose of using masks was to confine the electric field to certain region (window opening of mask) so that ion from the work piece would flow following the defined electric field path. Masks type and picture of mask were listed below:

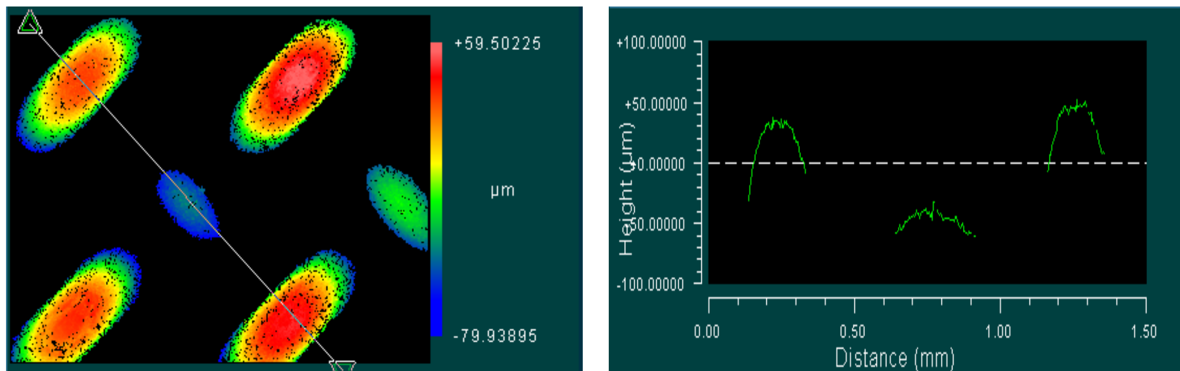

Figure 12 50PPI wire mesh.

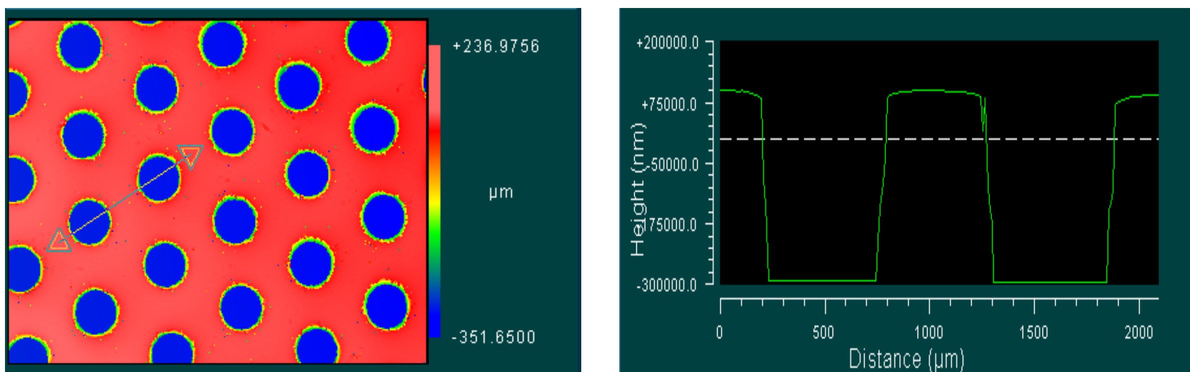

Figure 13 Perforated Stainless Steel with hole size of Ø = 570µm.

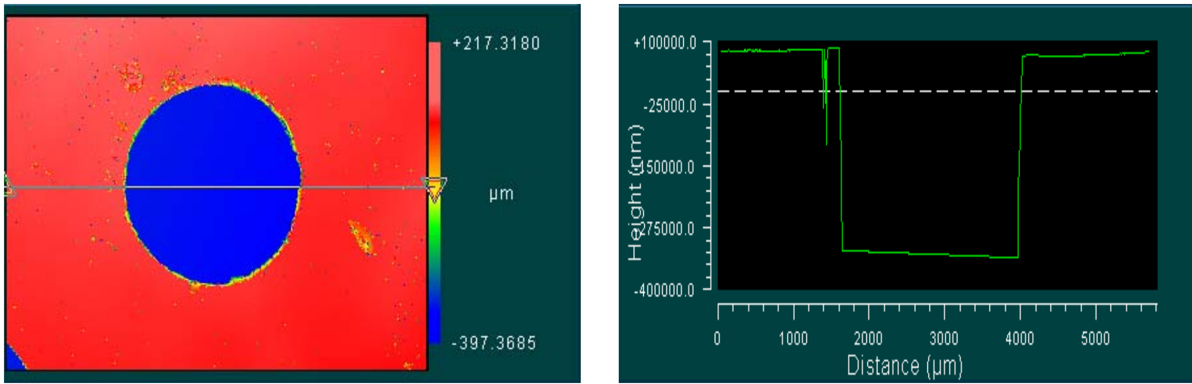

Figure 14 Polymer sheet with drilled single hole of Ø=2.2mm.

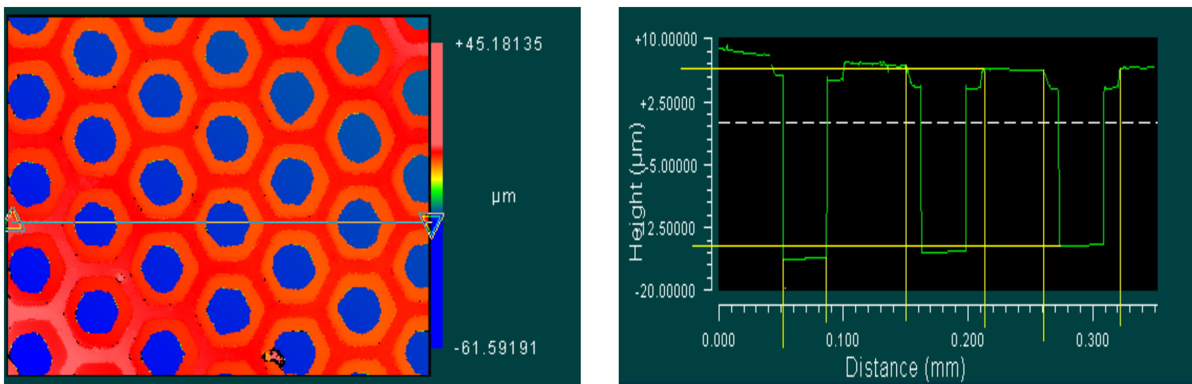

Figure 15 Transmission Electron Microscopy (TEM) mesh grid of 35µm window opening.

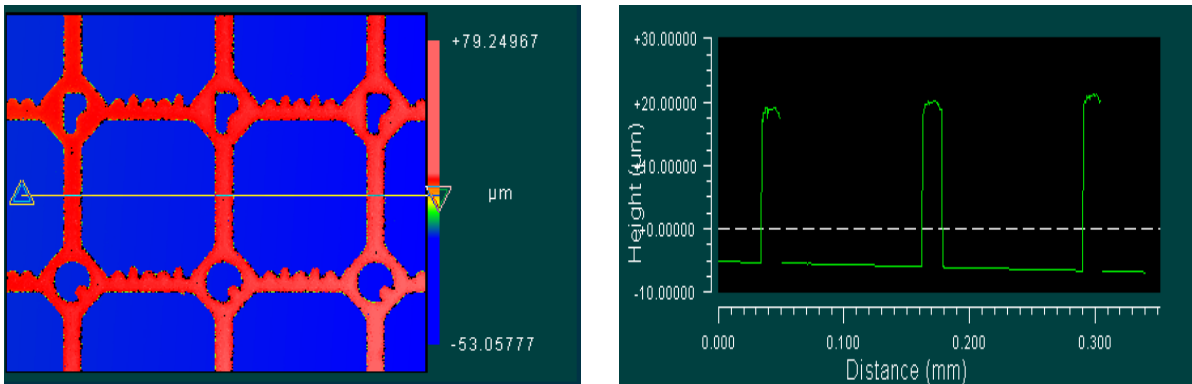

Figure 16 Transmission Electron Microscopy (TEM) mesh grid of 80µm window opening.

Copper TEM mesh with 35 µm and 80 µm windows opening used for this study were insulated by mixing sufficient amount of nail polish and acetone. The mixture was sprayed

on the surface of the mesh by using the air paint brush. Due to the window opening of the TEM mesh was such small that the mixture with low viscosity often times was clogging the window opening, compressed air was then applied within second to open the clogging area before the insulated layer became hard. Fluke® Multimeter was then used to check the conductivity of the material and making sure the dielectric behavior of the TEM mesh.

2.4 EQUIPMENT AND EXPERIMENTAL PROCEDURE

2.4.1 Equipments

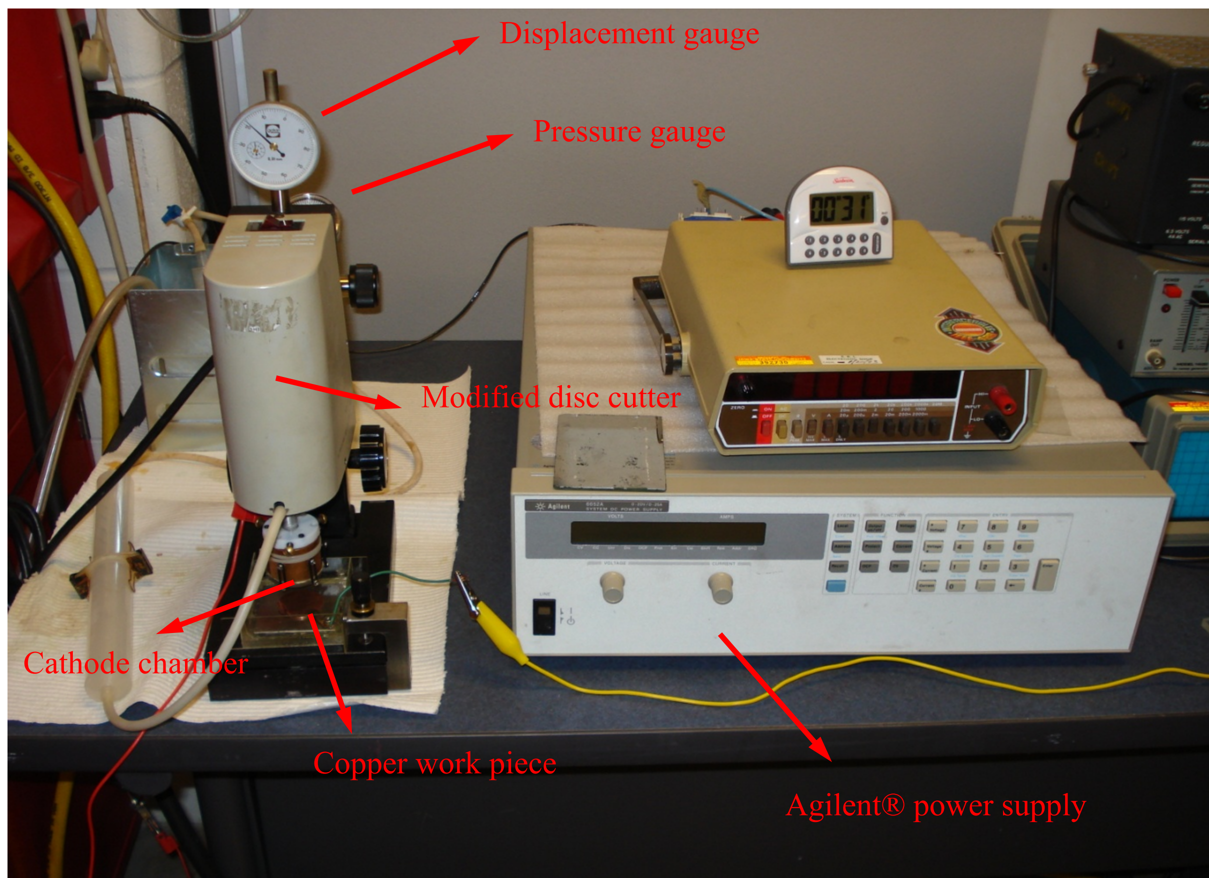

Figure 17 Experiment apparatus.

The experimental setup is constructed around a standard ultrasonic disc cutter, used to prepare TEM samples. A copper cylindrical cathode chamber (acted as negative terminal) is fitted to the disc cutter shaft. The Chamber has four holes (Ø = 5mm) on the bottom to allow exchange of ions. Two DuPont™ Nafion® Perfluorosulfonic Acid Polymer (Nafion membrane) of thickness 0.5mil and 2.0mil are utilized. The membrane is permeable to Cation (Cu^{2+}) from the Anode. The membrane is sealed to the cathode chamber by a double-sided tape and self locking Teflon ring. The Cathode chamber is connected via the shaft of the disc cutter to a vacuum system. A gate valve and pressure gauge dial are utilized to adjust the desirable amount of suction pressure. A flat basin is manufactured to hold the D.I. water and the anodic workpiece. The basin is made out of Plexiglas and adhered to a thick stainless steel plate to ensure planarity and flatness of the workpiece. The separation distance between the cathode chamber and the workpiece, is adjusted with a fine pitch screw and the high precision dial gage of the disc cutter. A highly stable power supply (Agilent 6652A) is used to apply either a voltage or current control to the electrochemical cell (Figure 17). A DC current clamped is used to monitor the circuit current.

A pulse generator, sweep generator, Insulated Gate Bipolar Transistor IGBT combined with Agilent power supply was used to perform chopped direct current experiment. The correct pulse duration (T_{on}) and pulse amplitude were observed on a Textronix oscilloscope.

2.4.2 Procedures

This section described the experimental procedure in detail starting from preparing the membrane to cleaning the surface of work piece after the experiment.

It was a crucial step to keep the Nafion membrane flattened and free from wrinkles. A piece of circular shape double sided tape with similar dimensions to the Teflon ring was first applied to the Teflon ring surface. The Nafion membrane (0.5mil) was protected by a layer of polymer at the front side of the membrane. The Nafion membrane (polymer free side) was then delicately adhered to another side of the tape. Tweezers was used along with delicate force to removed the polymer layer adhered to the membrane. Due to the fact that Nafion membrane has dependency on temperature and hydration (Solasi et al., 2007), an adequate amount of deionized water was sprayed on the Nafion membrane surface to start the relaxation behavior and remove wrinkling before starting the experiment. Curvature on the membrane was noticed due to the relaxation but it disappeared after membrane was attached to the bottom of cathode chamber with desirable mask attached between membrane and bottom of cathode chamber.

The cathode chamber was then taken under the fume hood to be filled with electrolyte. About 8mL of electrolyte was suctioned by a glass pipette into the cathode chamber. Detail descriptions regarding preparation of electrolytes are given in Section 2.2. Often time membrane was torn due to higher force being applied to attach membrane to the bottom of cathode chamber in the previous step. Check for membrane leakage was done before starting the experiment by observing the bottom of the cathode chamber whether the blue color electrolyte was leaking from any part of the membrane.

A T-shape Teflon cap designed for the cathode chamber was then inserted tightly. Three screws to hold the Teflon cap in placed with the cathode chamber was then fastened. Leakage of pressure was avoided by applying a fairly small amount of Corning® vacuum

grease to the inner surface of the Teflon cap where that was the place to be attached to the disc cutter's rod. Work piece was then loaded into the basin on the surface of the stainless steel piece. Fluke® multimeter was used to check the electrical conduction of work piece and stainless steel base. A reading of 0.1~0.3 Ω on the multimeter had shown a relatively good conductivity. Deionized water was filled in the basin to cover about 3mm above the work piece. After making sure Teflon cap was attached to the disc cutter's rod and work piece was in place, cathode chamber was brought down to touch the work piece via the disc cutter motion control mechanism. The gauge on top of the disc cutter showed certain value when bottom of cathode chamber touched the work piece. The gauge was then zeroed as a reference for full contact between the cathode chamber and the workpiece. Three lateral screws fixed at the outer diameter of the Teflon cap was meant to be tightened after the cathode chamber was in correct position (bottom of cathode chamber fully touching work piece) to ensure parallelism within the contact zone. Separation distance between two terminals was adjusted to a desirable value by the fine pitch screw (Figure 18) mounted to the stage of the disc cutter. While rotating the fine pitch screw, the separation distance was observed on the gauge on the top of disc cutter. Suction pressure was applied after the desirable separation distance was set.

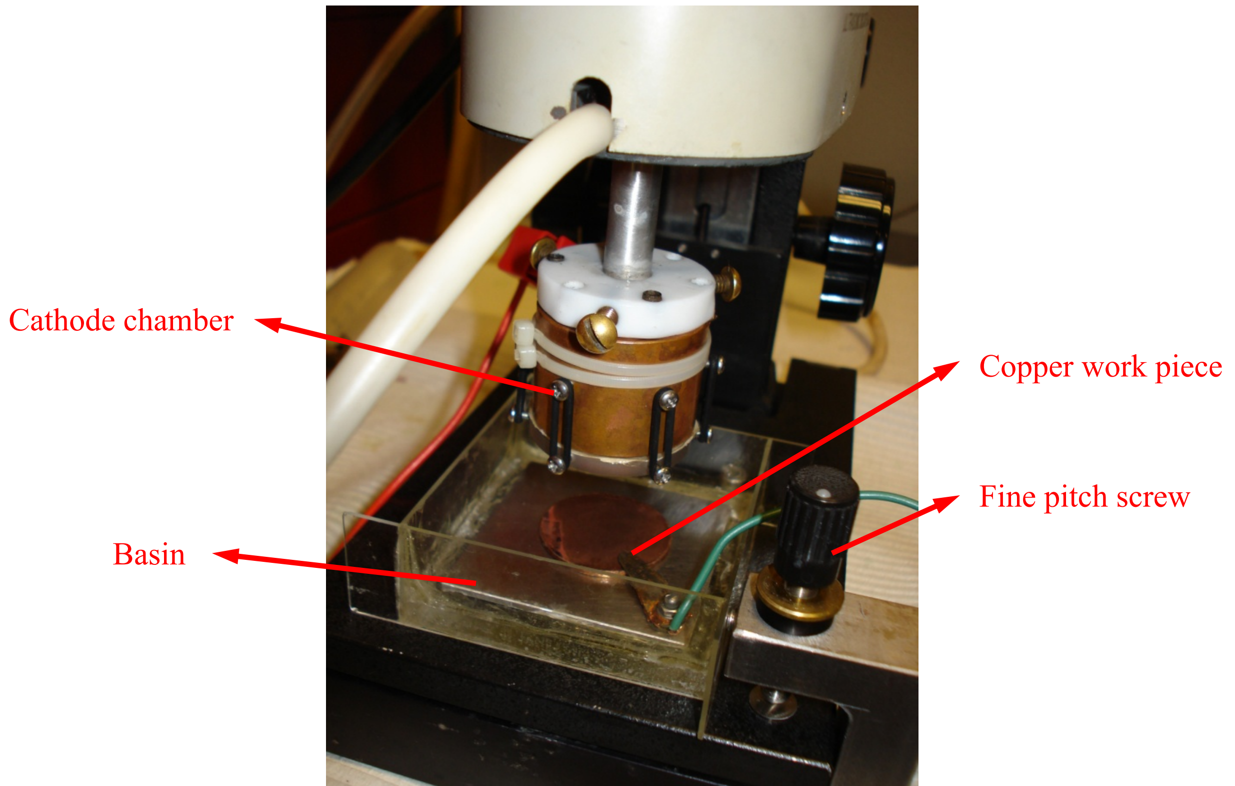

Figure 18 Cathode chamber and copper work piece placed in the basin.

Positive terminal from the power supply was connected to the work piece by an alligator clip attaching a wire linked from stainless steel base; negative terminal was connected to the cathode chamber by an alligator clip attaching a copper wire extended from the chamber. The desired voltage or current is set on the digital panel of the Agilent power supply and started timing the process. After certain amount of time, the experiment was stopped and removed alligator clips from both terminals. Cathode chamber was retracted to a higher position by rotating the dial on the disc cutter. Work piece was removed from the basin and sprayed with deionized water. Air gun was used to blow dry excessive amount of water and workpiece was saved in the vacuum chamber to prevent the formation of copper oxide film.

2.5 IMAGING ANALYSIS PROCEDURE

Material removal rate (MRR) was the ultimate parameters to compare different experiment parameters settings such as suction pressure applied, voltage or current applied, variation of separation between two terminals and concentration of electrolytes used.

The pattern on workpiece was analyzed using non-contact 3D surface profilometer (Zygo® NewView6K). The core technology used by this profilometer was white-light surface interferometry. A lowest magnification scan (5X) was acquired of the embossed pattern on the surface of workpiece to provide an overview of the patterned area. Images on random spots on the patterned area were then taken with higher magnification settings (50-100X) in order to get a detailed profile of the embossed pattern width and depth. The raw data are stored before further data analysis and reduction. Several measurements (about five) were conducted on each embossed pattern due to the spatial variability of MRR within the pattern. The average of these measurements was used to set a level for the MRR for each case.

CHAPTER 3: EXPERIMENTAL RESULTS & DISCUSSIONS

Summary of the experimental data for each of the methods are presented here. A typical pattern profile of each case is also presented. Variation of the MRR and pattern accuracy are examined with several of the process parameters, including applied voltage, standoff distance, applied suction pressure (where applicable), exposure time, duty cycle of chopped DC voltage (CDC) as well as the role of electrolyte concentration.

3.1 DIRECT CONTACT MASK-MODULATED ELECTRIC FILED PRINTING

3.1.1 TEM mesh with 80μm window opening

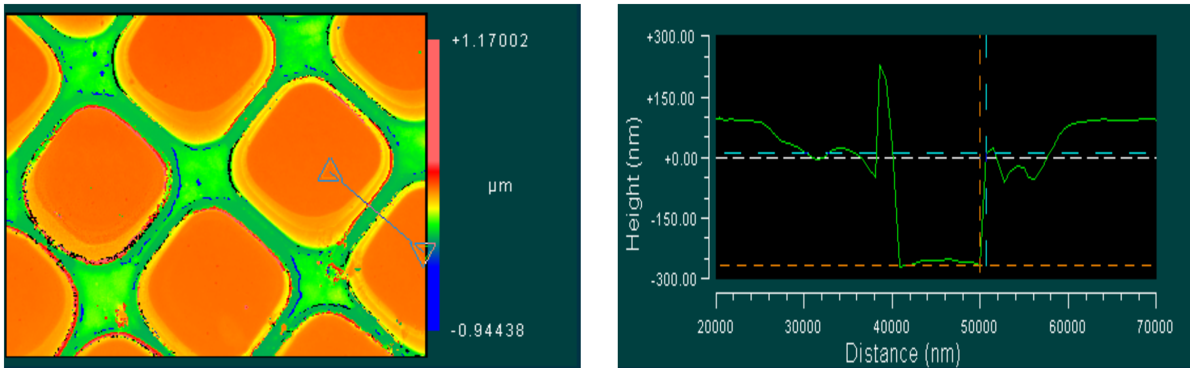

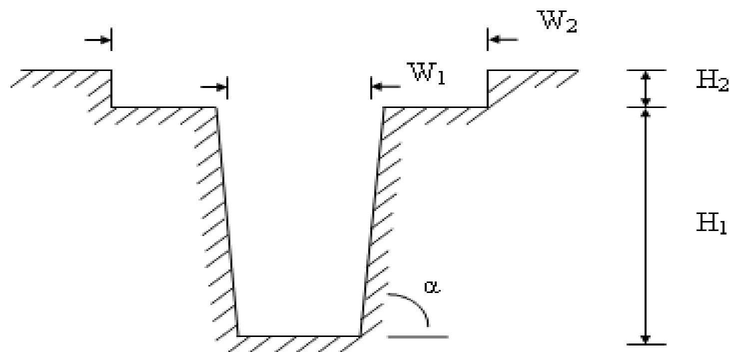

Figure 19 Profilometer images of printed pattern by 80µm window opening mesh. The sketch gives a brief view of how dimensions are measured across the printed pattern. (CDC voltage, pulse duration = 0.02/200µsec., exposure = 10sec., electrolyte = 0.01M H_2SO_4 + 0.5M $CuSO_4$)

The utilized mask is 3mm in diameter with a square feature of 100µm periodicity. The opening was 80µm and the ligament width is about 20µm. There were also finer features on the vertical ligament with 8µm dimensions. Since this mask is use in direct contact, the fill ratio of the ligament was more important than the opening. The fill factor for this mask is about 36%.

3.1.1.1 Imprinting under voltage control (CDC)

This set of experiments was conducted under voltage control setting. For the entire data set, the total current was within the power supply sensitivity (about 10mA). Such level would provide a current density of about 400mA/cm^2. The applied voltage was varied between 2-5V, to examine its effect on printed pattern accuracy and topology. Figure 20 shows the role of the applied voltage on printed pattern angle, α, pattern depth, H_1 and width W_1. In addition, it was observed that the imprinted pattern has a wider entrance, W_2 which space a depth of H_2. The MRR (given by H_1) started after reaching a threshold voltage of about 2V (Figure 20(a)). Such threshold could be understood as the needed voltage to overcome the electric double layer on the surface. Beyond the threshold voltage, a linear dependence of the MRR on the applied voltage was observed. It could be attributed to the increased oxidation rate of the Cu^{2+} ions with the applied electric field. Except for the first data point, the trench width increased from 40 to 60% of the initial electrode thickness, as the applied voltage is increased (Figure 20(b)). The measured side wall angle was quite shallow,

in the range of 5-15° (Figure 20(c)) and was increasing with the applied voltage. However, when compared to the trench width, the entire slope of the trench wall does not occupy more than 10% of the trench width. The low angle of the printed side walls throughout this set of experiment shows that the machining precision has to be further improved in order to approach close to 90° trench walls. Figure 20(d) shows the variation of the trench entrance with the applied voltage. For a distance of about 12-17% of the total trench depth, a wider zone, W_2 which is of about twice the ligament width was eroded. While H_2 showed a mild dependence on the applied voltage, W_2 was almost independent of the applied voltage. Notice that the ligament width of the original TEM mesh itself is 20μm and width large at voltage settings of 2V to 5V gives an average width large at approximately 50μm (Figure 20(e)). Such results points to the need of full numerical simulation of the complex electric field underneath the electrode. Moreover, the lateral dispersion of the electric field with the Nafion membrane has to be addresses, in order to understand the wide entrance generated at the entrance of the trench pattern. Moreover, the role of the side walls of the electrode has to be understood in order to elucidate on the width of the printed pattern.

(a)

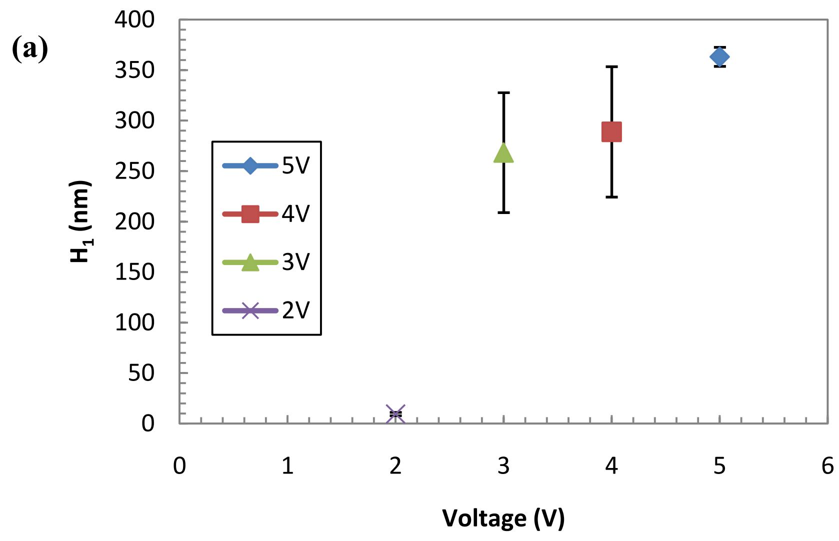

(b)

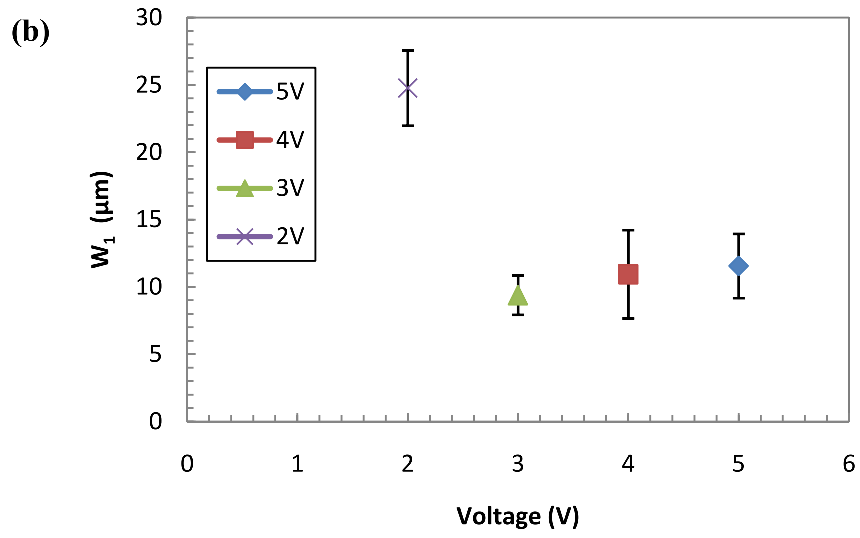

(c)

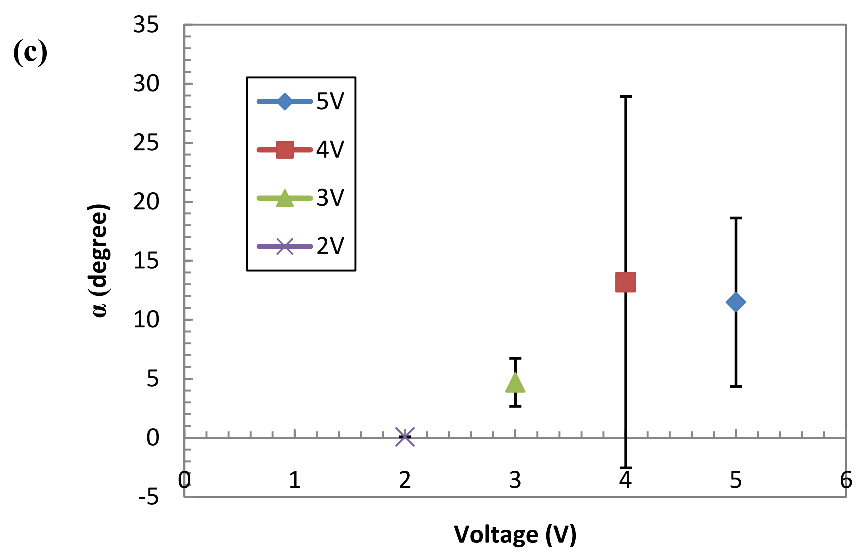

(d)

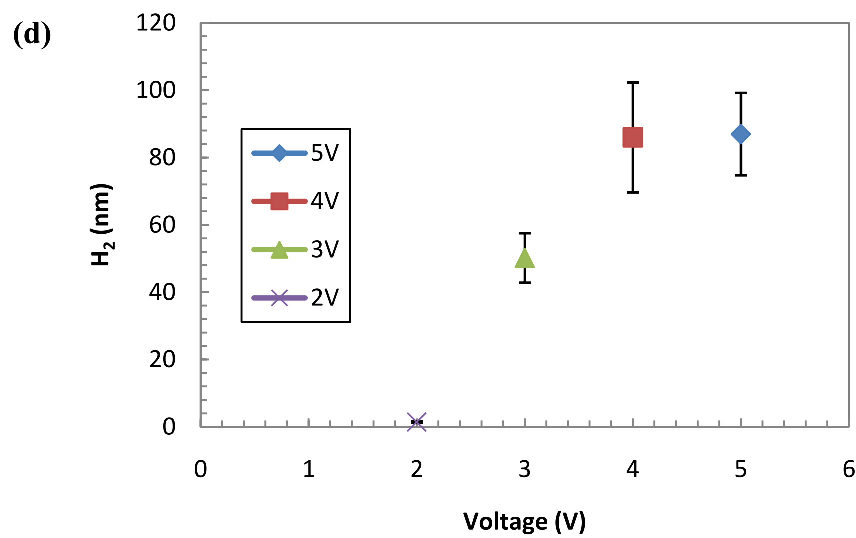

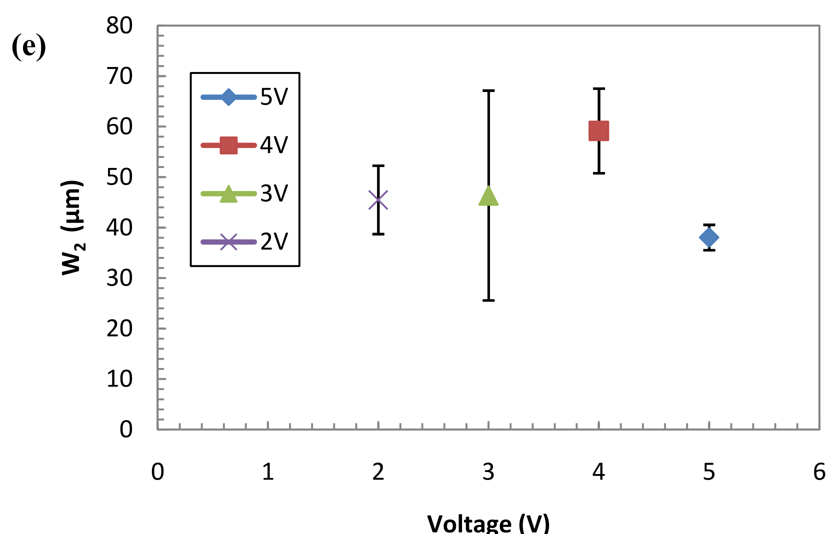

Figure 20 Analysis on the machining accuracy of the printed pattern with respect to different voltage applied. (a) H_1 (b) W_1 (c) α (d) H_2 (e) W_2 of the pattern. (CDC voltage, pulse duration = 0.02/200µsec., exposure = 10sec., electrolyte = 0.01M H_2SO_4 + 0.5M $CuSO_4$)

3.2 NON-CONTACT MASK MODULATED ELECTRIC FIELD PRINTING

3.2.1 Wire Mesh

This data set is one of the early exploratory ones where a simple wire mesh was used as a proof of the concept. The utilized 50PPI mesh was used without any insulation. By comparing the topography of the mask and the printed pattern, it was found that the imprinted patterns matched the vertices of the mask as shown in Figure 21(c), (d). The wire mesh has two different levels of its intersecting wire vertices due to the winding direction. It is evident that the mesh vertices acted as a focal point to focus the electric filed through the Nafion® membrane. Thus, the contact area if the vertices are measured from the surface topography of the wire mesh in Figure 21(a). The estimated fill ratio of the mask is about 5%. The mask has a diameter of 18mm. This data set is however provide some insight on the role

of the applied current, wherein very large current density based on the vertices area was applied (5-10A/cm^2) to imprint patterns with more than 10μm depth. Moreover, the standoff distance was quite large (in the range of 100-200μm) for this set of experiment.

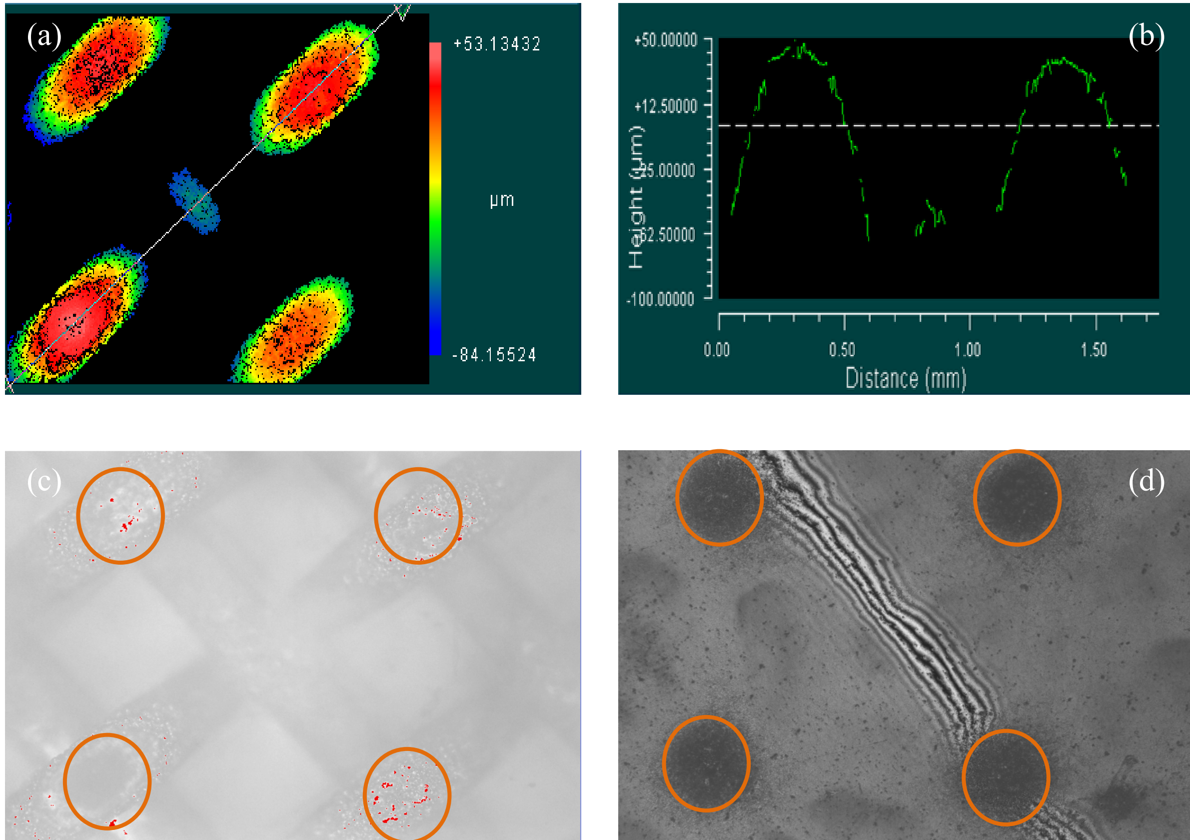

Figure 21 (a) Topography and (b) cross-sectional profile of the 50PPI wire mesh. (c) The 50PPI wire mesh and (d) printed pattern on the copper work piece. Notice that rings in (c) are added on top of the vertices in order to compare to the printed patterns in (d). (Mag.=5X)

This data set elucidates the possibility of using very high density current if a long standoff distance is maintained. Such long standoff distance would help in dissipating any joule heating effect as well as maintain the hydration of the membrane.

3.2.1.1 Imprinting under current control (DC)

As current is increased from a lower level to higher level, the amount of Cu^{2+} ions transport through the Nafion membrane at a fixed exposure time will be increased. Seemingly, MRR has increased 55% when applied current varies from 0.7A to 1.15A (Figure 22). This is equivalent to a change of the current density from 5500mA/cm^2 to 9000mA/cm^2. Such current level was supported since the mesh had a very thick gage. The average was not recorded for this set of experiment. Due to the ambiguity of the exact conductive area, the average current density over the entire mask is about 275mA/cm^2 to 450mA/cm^2.

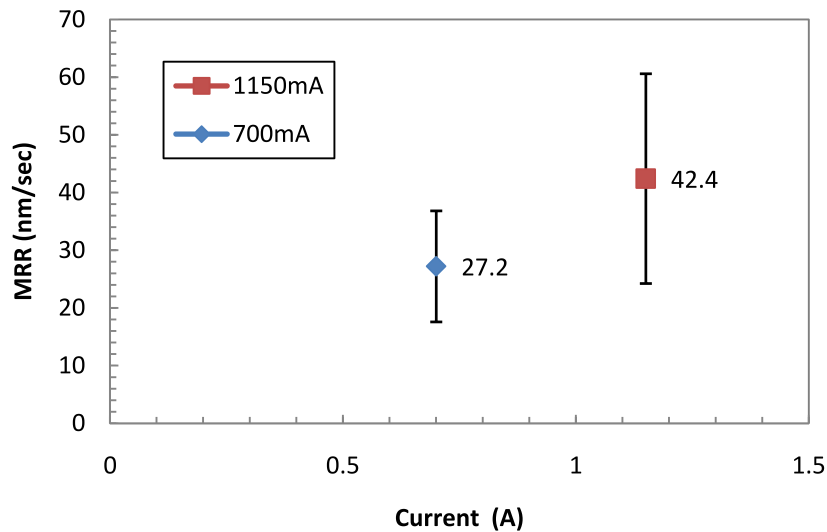

Figure 22 50PPI mesh, material removal rate versus current variation. (DC voltage, standoff distance = 200µm, exposure = 300sec., electrolyte = 1.80M H_2SO_4 + 0.25M $CuSO_4$)

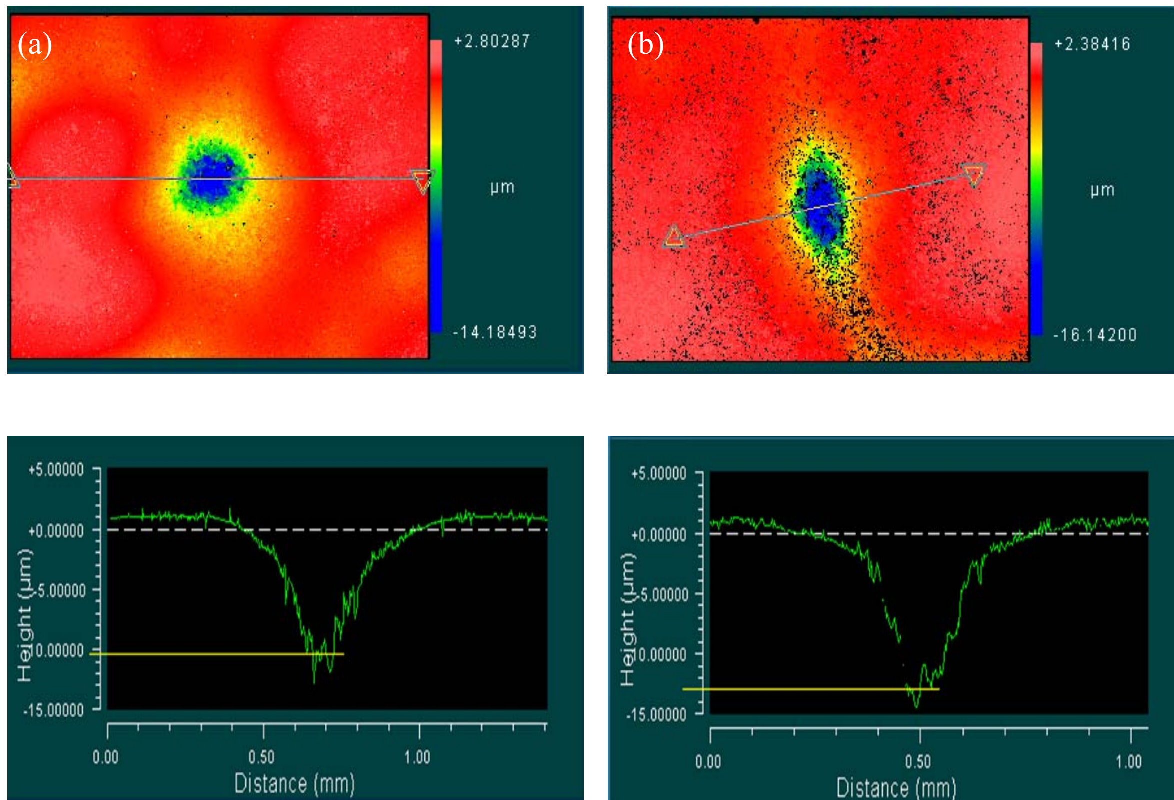

Figure 23 Wire mesh, 50PPI mask results for the imprinted pattern (a) I = 700mA (b) I = 1150mA. (Mag=10X) (DC voltage, standoff distance = 200µm, exposure = 300sec., electrolyte = 1.80M H_2SO_4 + 0.25M $CuSO_4$)

3.2.2 Perforated Stainless Steel

The perforated stainless steel mask has a triangular hole array of 570µm diameter and a triangular pitch of 1170µm. The opening ratio is about 19%, which would be used for current density calculation. The mask is well insulated before usage. The role of the mask here is to confine the electric field to the opening holes only. Thus, the mask opening ratio would be used for the electric current density. The mask diameter is 16.9mm.

3.2.2.1 Imprinting under current control (DC)

Figure 24 summarizes the role of the applied current on the MRR. An increase of about 17% in MRR was observed for a change of about 80% increase in the applied current. The average current density based on the opening ratio is about 2470mA/cm^2 to 4425mA/cm^2. Figure 25(a), (b) shows that the imprinted hole has a depth, H_1=1.95µm, W_1=725µm and very inclined side walls of about 1°. The ratio of the imprinted pattern diameter to the hole opening is about 127%. The wall inclination occupies about 20% of the imprinted hole diameter. It is remarkable to notice that the width of wall inclination is of the same order of the standoff distance (150µm). It is obvious that significant electric field divergence has taken place here. Additional investigations are needed to understand the role of the standoff distance as on the conformity of the electric field to the original opening of the mask.

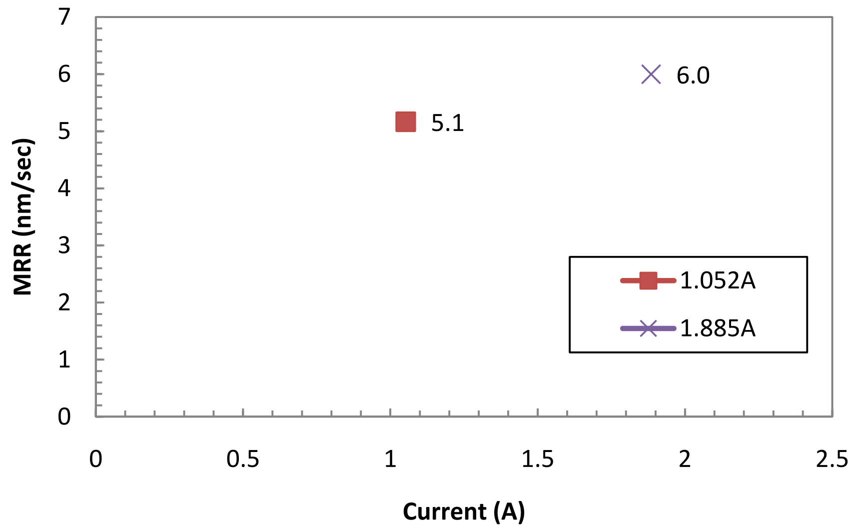

Figure 24 Perforated stainless steel 570µm, MRR versus current variation. (DC voltage, standoff distance = 150µm, exposure = 300sec., electrolyte = 1.80M H_2SO_4 + 0.25M $CuSO_4$)

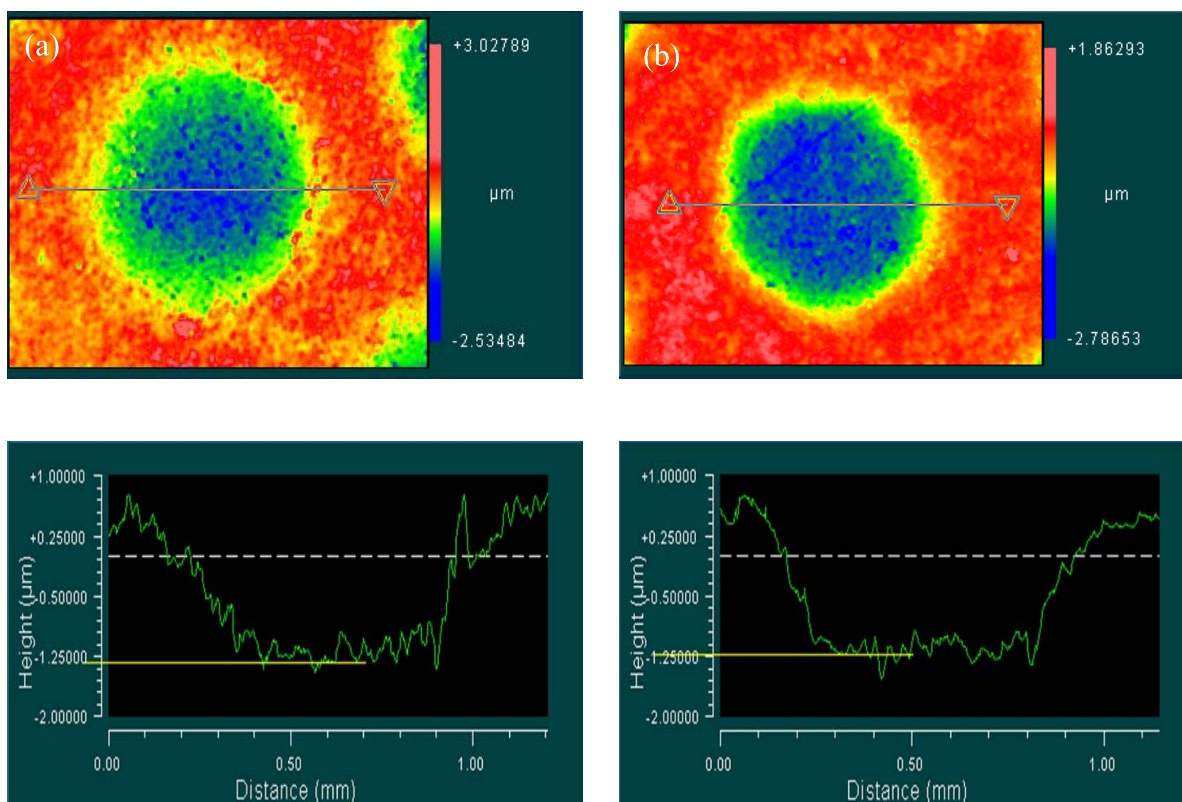

Figure 25 Perforated stainless steel 570µm 2D surface render at 5X. (a) I = 1.052A (b) I = 1.885A. (DC voltage, standoff distance = 150µm, exposure = 300sec., electrolyte = 1.80M H_2SO_4 + 0.25M $CuSO_4$)

3.2.2.2 Imprinting under current control (CDC)

This data set is among the early trial to utilize chopped DC electrochemical cell. Many issues code be associated with this data set such as the limitation of duty cycle to several hundred hertz, attainable by the IGBT at high current. The objective of using CDC is to examine the role of the duty cycle on the accuracy of the imprinted pattern by limiting the time constant for any lateral diffusion if it exists, in contrast with the bad results from DC-printing, shown in (Figure 25(a)(b)). In addition, it is contemplated that if the CDC can

disturb the formation of the electric double layer, and thereby enhance the dissolution rate of the copper ions, the MRR could be increased.

Figure 26 summarizes the dependence of the MRR on the applied current. The data show almost no-correlation with the amplitude of the electric current. However, the MRR was about 2-3 times those achieved under DC only. The imprinted pattern profile is shown in Figure 27. The imprinted pattern is a donut-like shaped, rather than a blind hole. The pattern has an outer diameter of about 850μm and an inner diameter of approximately 570μm (similar to the hole opening diameter of the mask). In essence, we were getting a circular trench of about 150 μm. It is suspecting the holes inner surface of the perforated sheet are not well insulated, and thus are acting as a vertical ring electrode. More detailed modeling, accounting for such geometry is needed.

The increase in the MRR points to the possibility of an existence of a threshold that has to be overcome to induce the material removal. Moreover, it is also important to note the long cycle duration relative to the pulse duration (6.25/400msec.). It is possible that there is possibility for charge accumulation during the pulse on-time. These charges may continue to affect the copper dissolution during the long pulse off-time period, and thereby become in dependent of the amplitude of the applied current. Therefore, the relatively high MRR could be coming from a secondary effect such as charge accumulation at the mask/Nafion® membrane interface.

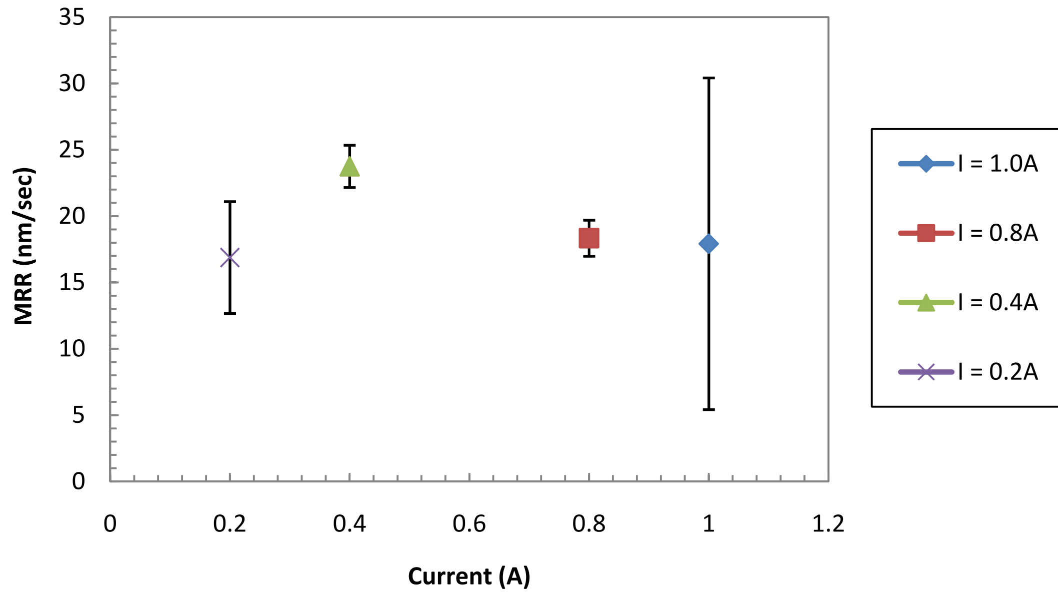

Figure 26 Perforated stainless steel 570µm, MRR versus current variation. (CDC voltage, standoff distance = 75µm, pressure = 15inHg, pulse duration = 6.25/400msec., exposure = 60sec.., electrolyte = 1.80M H_2SO_4 + 0.25M $CuSO_4$)

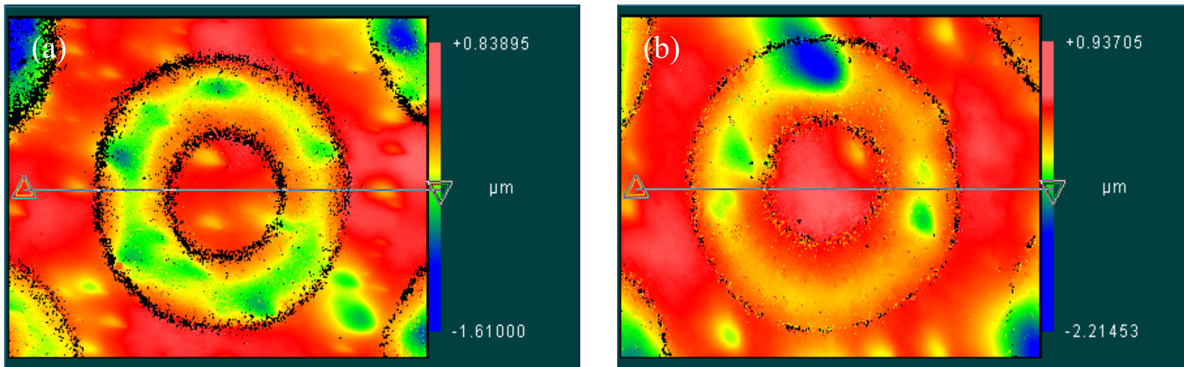

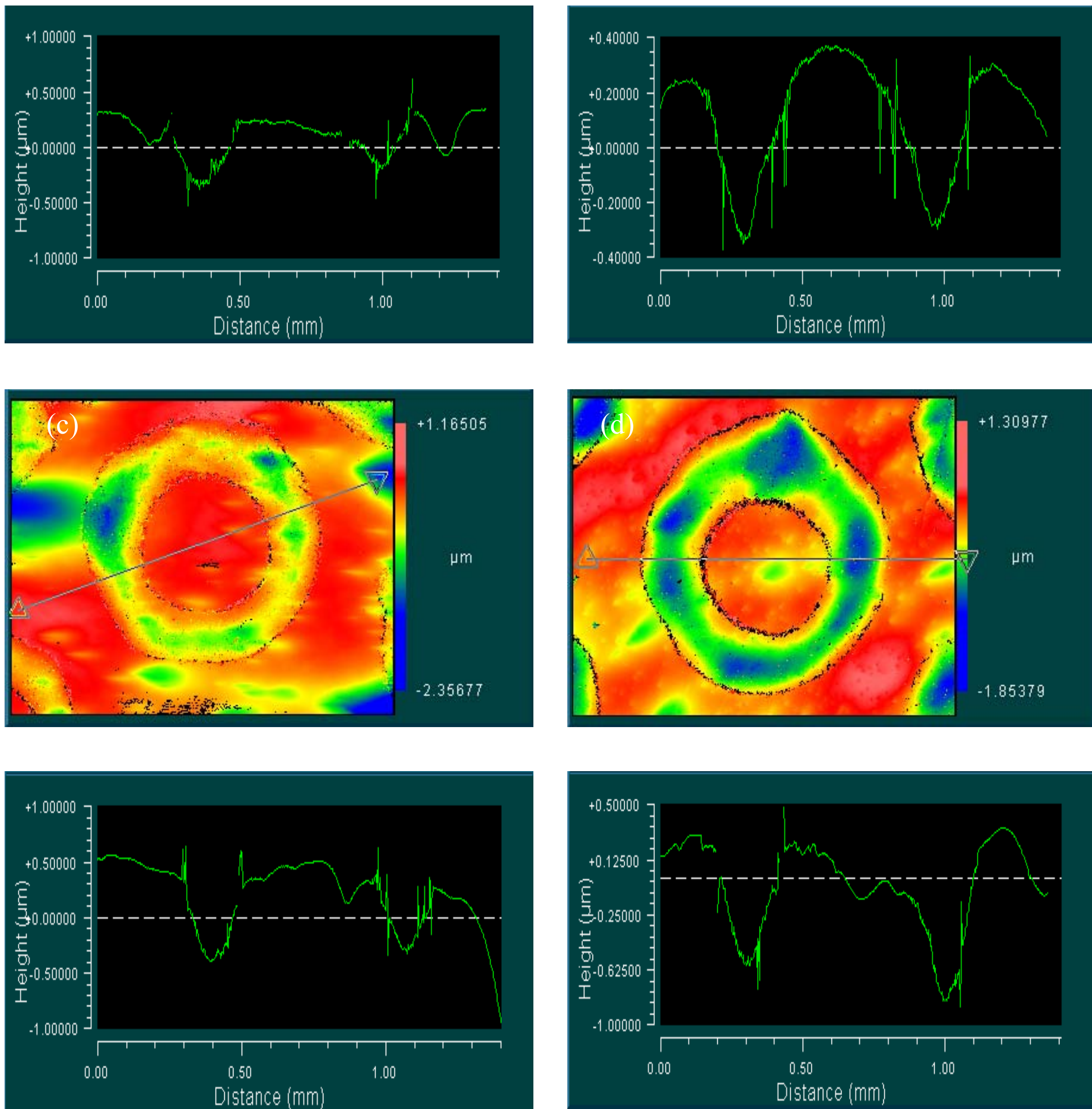

Figure 27 Perforated stainless steel 570µm 2D surface render at 5X. (a) I = 1.0A (b) I = 0.8A (c) I = 0.4A (d) I = 0.2A. (CDC voltage, standoff distance = 75µm, pressure = 15inHg, pulse duration = 6.25/400msec., exposure = 60sec.., electrolyte = 1.80M H_2SO_4 + 0.25M $CuSO_4$)

It was noted by Kock et. al. (2002) that the MRR was increased by increasing the pulse duration. To reconcile such finding we performed several other tests with the same

testing conditions, except varying the pulse duration while keeping the total pulse period constant. It can be seen in Figure 28 that MRR vary nearly linearly with increasing T_{on}.

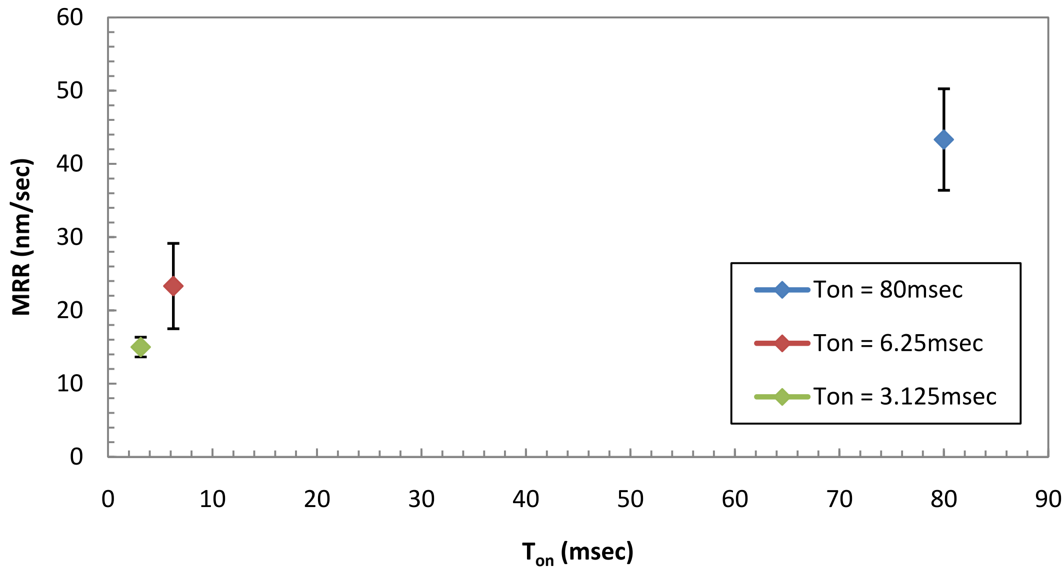

Figure 28 Perforated stainless steel 570µm, MRR versus total pulse duration. (CDC voltage, standoff distance = 75µm, pressure = 20inHg, Current = 1.3A, pulse period = 400msec., exposure = 60sec., electrolyte = 1.80M H_2SO_4 + 0.25M $CuSO_4$)

3.2.2.3 Electrolyte Concentration Variation

The role of electrolyte concentration and conductivity is explored with the perforated mask and DC-voltage control.

Table 3 shows the conductivity of the electrolyte at different concentration levels. For this particular data set, the entire electrode chamber was well insulated. The electrode distance was kept at 1mm from the mask, as shown in the sketch of Figure 30. The experimental parameters were kept constant at 0.5V, 60sec. exposure, 20µm standoff distance and 1inHg vacuum pressure.

Concentration of H_2SO_4, M	Conductivity, mS/cm
0.01	33
0.05	43
1.0	676
1.8	1207

Table 3 Electrolyte conductivity with at different concentration levels of H_2SO_4.

Figure 29, shows the role of electrolyte concentration and conductivity on the MRR. The MRR sharply increased by 300% when the concentration of H_2SO_4 increases from 0.01Molar to 0.05Molar. However, at 1Molar the MRR increased by 25% from its value at 50mMolar. Thus, copper ions dissolution rate becomes limited by the kinetics of the double layer at the workpiece interface. Moreover, the role of $CuSO_4$ is also examined. Its main role is to replenish the electrolyte with Cu^{2+} ions and maintains its conductivity as well as reduces the hydrogen gas formation. Reducing the concentration of $CuSO_4$ to half of the previous amount decreases the material removal, given that concentration of H_2SO_4 is 0.8Molar higher than 1.0Molar. This shows that $CuSO_4$ in the electrolyte not only is to reduce the hydrogen gas formation, but rather to maintain the concentration of Cu^{2+} in the electrolyte and thereby the reaction rate. Printed pattern at 1.80M H_2SO_4 has poorer surface quality compare to the lower acid concentration.

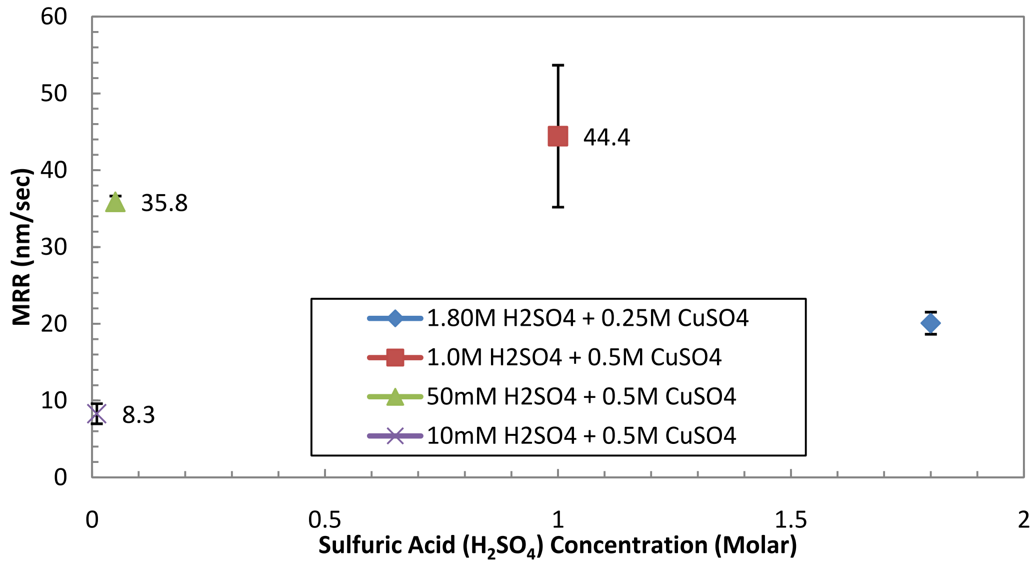

Figure 29 Perforated stainless steel 570µm, comparison of MRR at different electrolyte concentrations. (DC voltage, Insulated perforated stainless steel hole, insulated cathode chamber with added round electrode, P = 1inHg, standoff distance = 20µm, exposure = 60sec.)

3.2.2.4 Roll of the Cathode position

For this data set, the entire cathode chamber was completely insulated with nail polish, except for the two electrodes at different heights, as well as the two holes with no electrode at all, as shown in Figure 30. The copper round shape electrode (diameter of Ø = 3.5mm) was located 1mm from the bottom of the cathode chamber; the copper rectangular shape electrode (5mm X 6.7mm) was placed 5mm from the bottom of cathode chamber. The electrolyte concentration was kept at the lowest employed level of 0.01M H_2SO_4 + 0.5M $CuSO_4$. Other experimental parameters were kept constant at 0.5V, 60sec. exposure, 20µm standoff distance and 1inHg vacuum pressure. Figure 31 sketch shows how printed pattern angles, widths and heights were measured from the profilometer image.

The imprinted profile characteristics are summarized on (Figure 32). The closer the electrode from the mask and the Nafion® membrane, the higher the MRR (H_1), lowest pattern dispersion (W_1) and the most confined wall angle. For the 1 and 5mm separation distance, W_1 was about 16% more than the mask hole diameter. For the no direct electrode case, W_1 was about 22% more than the mask hole diameter. Thus the location of the electrode does not have a great effect on either the wall angle or pattern dispersion. However it has the greatest effect on the MRR. These numbers has to be compared with the first exploratory data set shown in Figure 24-Figure 25 to contrast the quality of the imprinted features.

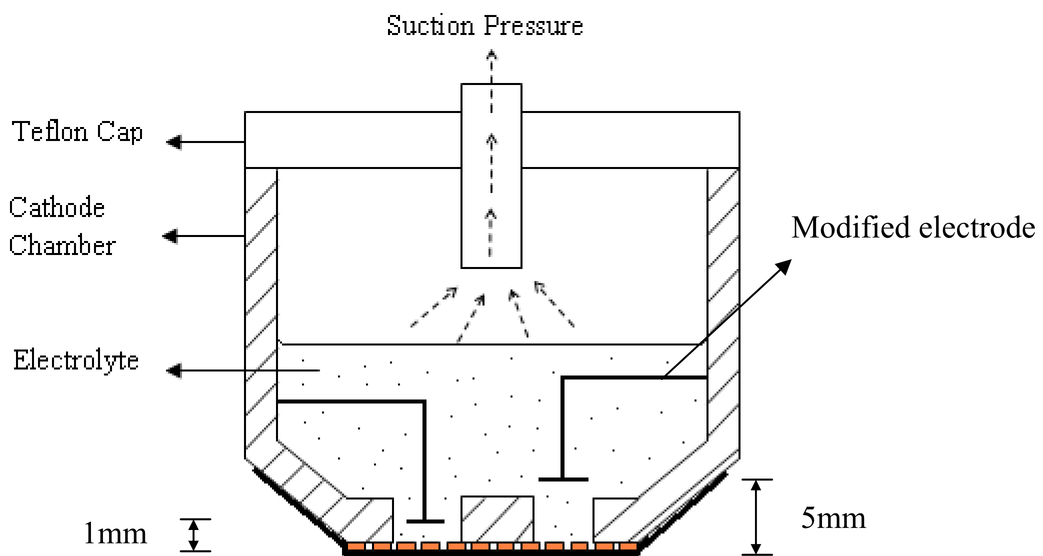

Figure 30 Modified electrode in the cathode chamber.

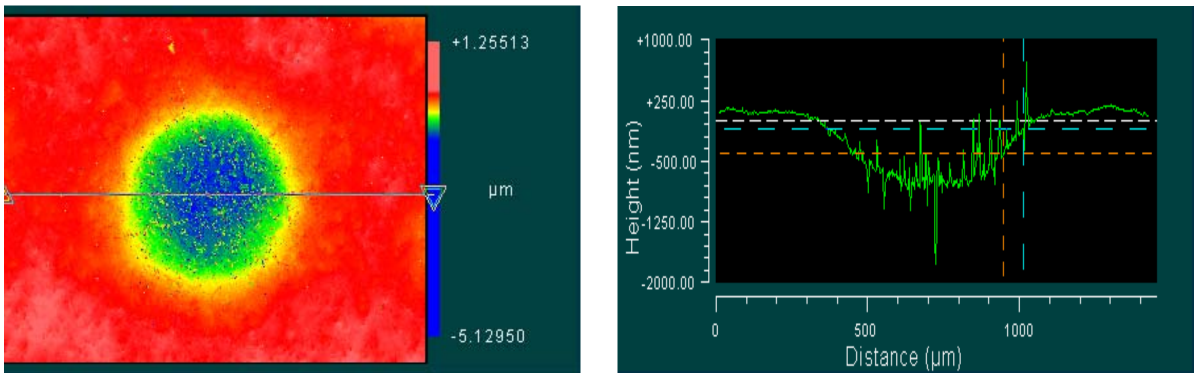

Figure 31 Sketch to show how dimensions were measured from printed pattern.

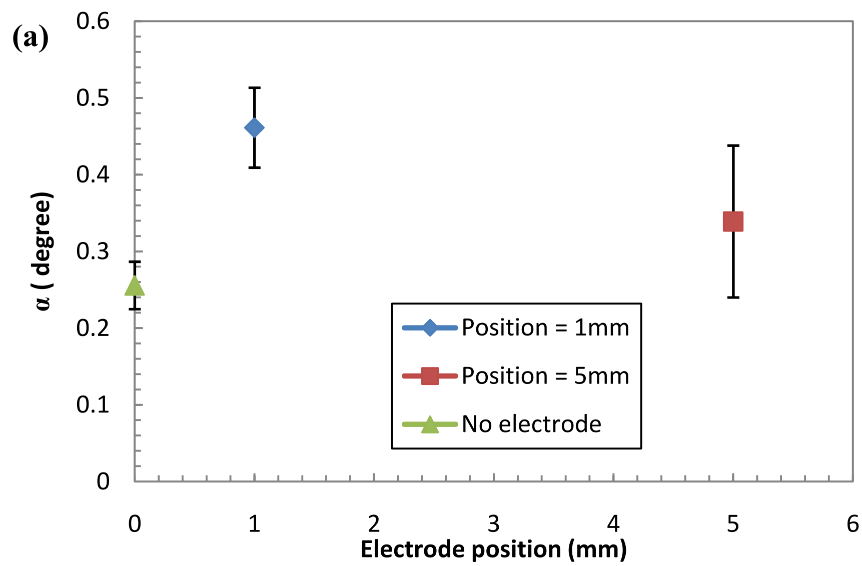

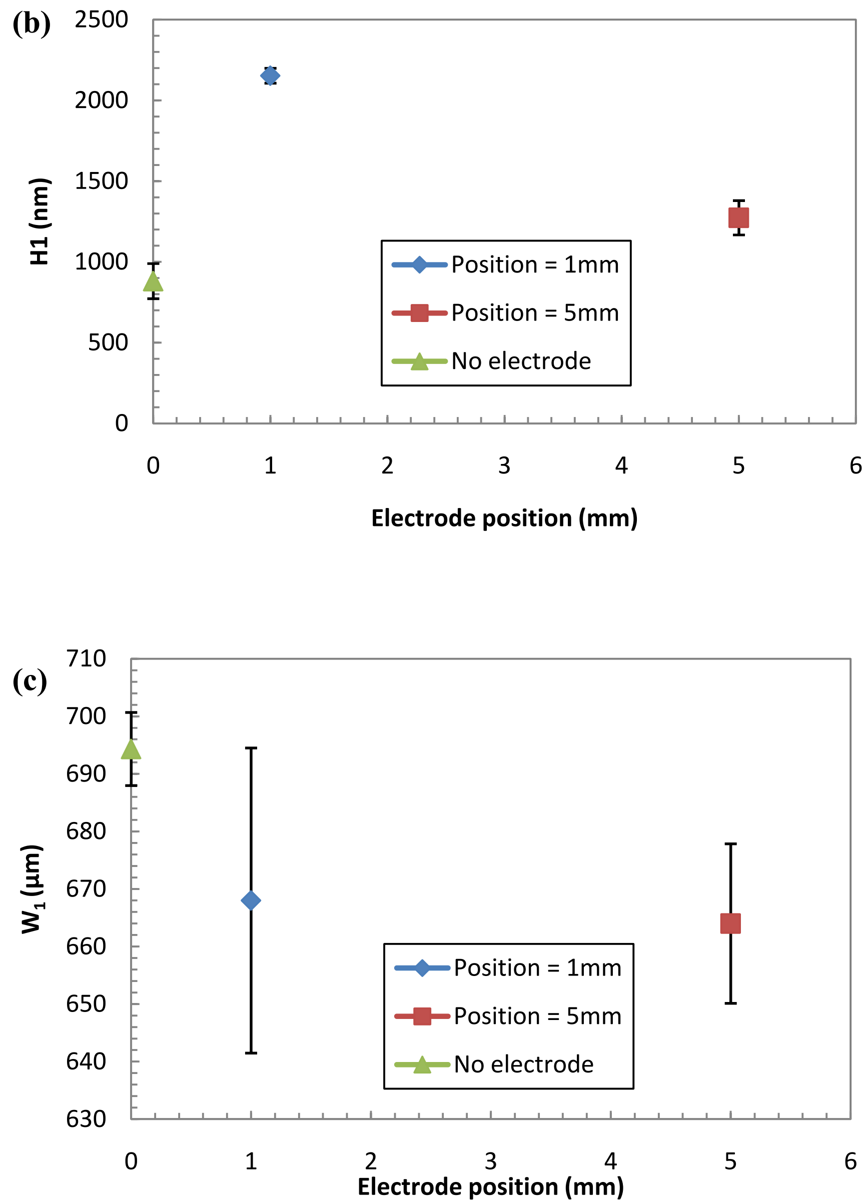

Figure 32 Perforated stainless steel 570µm, comparison on the (a) printed pattern side wall angles, α (b) printed pattern depths, H_1 and (c) printed pattern widths, W_1 at three different electrode positions. (DC voltage, Insulated perforated stainless steel hole, insulated cathode chamber with added rectangular electrode, P = 1inHg, standoff distance = 20µm, applied voltage = 0.5 V, Electrolyte = 0.01M H_2SO_4 + 0.5M $CuSO_4$, exposure = 60sec.)

3.2.3 Polymer mask with a single 2.2 mm hole

This idealized mask is utilized to study the role of the suction pressure on the membrane curvature and the possibility of pattern reductions. Moreover, the role of standoff distance from the workpiece on the imprinted profile quality is also examined.

3.2.3.1 Roll of applied pressure

Varying the applied suction pressure will change the curvature of the Nafion membrane. The objective of modulating the curvature of membrane is to examine the possibility of focusing the electric field to induce pattern reduction on the workpiece. A non-conductive polymeric mask is used to reduce the ambiguity associated with conductive one in identifying the electric field lines. The experiment was conducted under current control CDC with fixed experimental parameters (50mA, 15sec. exposure, 10μm standoff distance and 0.5/50msec. duty cycle). Figure 33 shows that the height averaged MRR does not depend on the variation of the curvature of the Nafion membrane. Modulation of membrane is not that obvious at lower suction pressure settings and thus the focusing effect is not obvious as seen in Figure 34(a) and (b). As the suction pressure increase further from 0.5inHg to 4inHg, a donut-shape pattern started showing possibly the focusing effect. There are many ways to physically understand such pattern. One way is to argue that the curved membrane would have a larger standoff distance at its center compared to the edge. Thus the electric field at the workpiece would be modulated. Another way, is to argue that the membrane curvature is slightly elliptical in shape with two loci. If the curvature of the membrane would indeed focus the electric field, then the formed donut shape is a direct

outcome of such elliptical shape. Such speculations need detailed analysis of the interaction between the Nafion® membrane and the electric field.

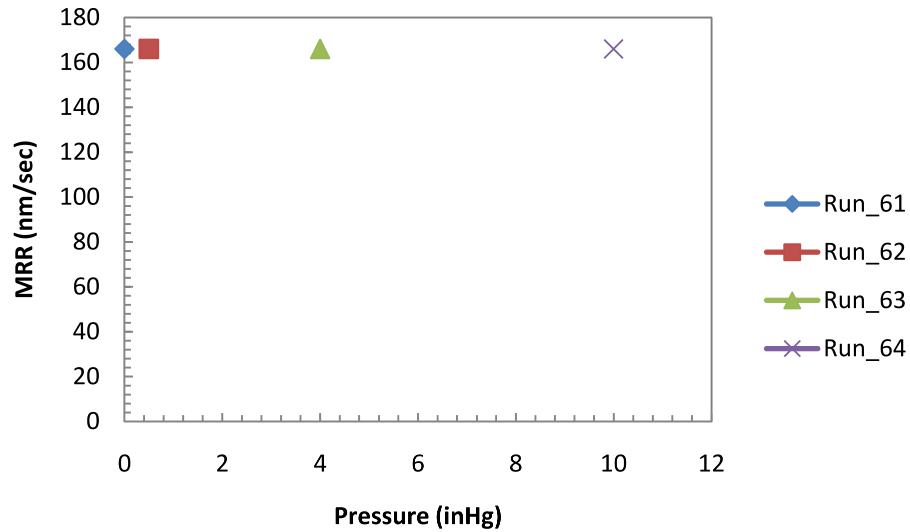

Figure 33 Polymer sheet with single drilled 2mm hole, material removal rate versus pressure variation. Experiment parameters: (CDC voltage, standoff distance = 10µm, current = 0.05A, pulse duration = 0.5/50msec., exposure = 15sec., electrolyte = 1.80M H_2SO_4 + 0.25M $CuSO_4$)

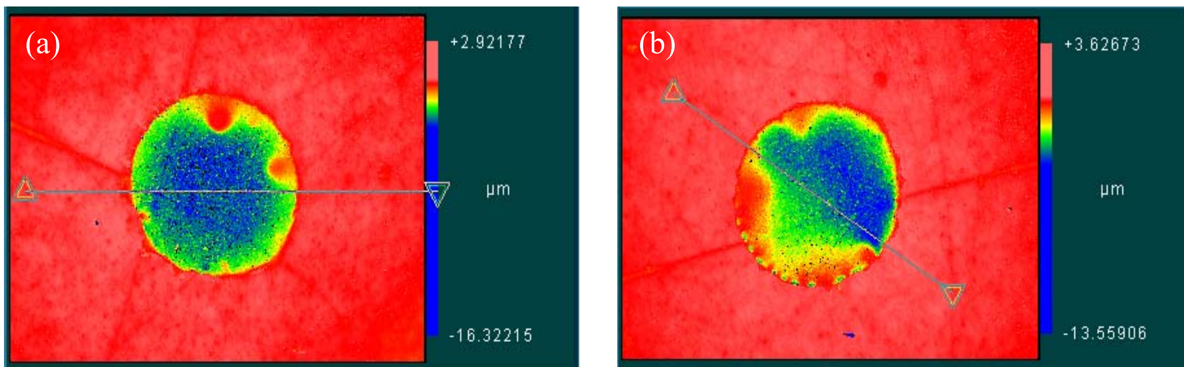

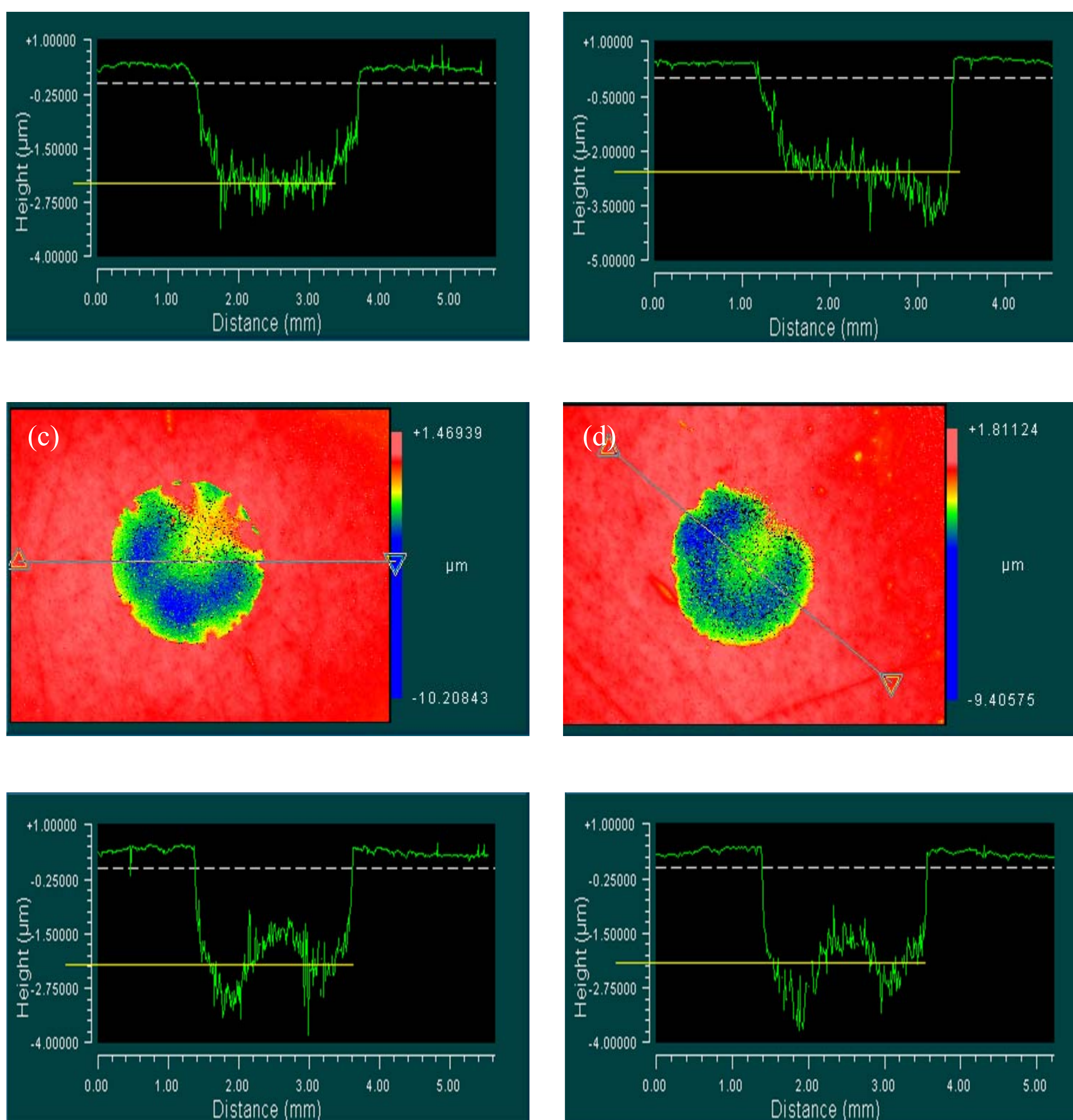

Figure 34 Polymer sheet with single drilled 2mm hole, comparison of pressure variation at 1.25X. (a) P = 0inHg (b) P = 0.5inHg (c) P = 4inHg (d) P = 10inHg. (CDC voltage, standoff distance = 10µm, current = 0.05A, pulse duration = 0.5/50msec., exposure = 15sec., electrolyte = 1.80M H_2SO_4 + 0.25M $CuSO_4$)

3.2.3.2 Roll of standoff distance

The standoff distance between the cathode chamber and the anode workpiece was varied between 10-60µm, while keeping all other experiment parameters constant. The experiment is done under constant voltage of 3V, 15sec. exposure, pulse duration = 0.5/50msec.. As shown in Figure 35(a), a decay of the MRR is observed with the increase of the standoff distance. The increase of the standoff distance increases the electrical resistance in the system increases, and thereby lesser amount of Cu^{2+} ions are transferred from the workpiece. The width of the printed pattern did not change significantly with the standoff distance with a 9% increase above the mask hole. However, the data for the 10µm standoff distance deviates extensively from the mean trend. It seems that this data point is an outlier. Similar varying standoff distance experiment was done by utilizing 35µm TEM mesh in Section 3.3.1.2 and further validated the 10µm data point was not following the mean trend. The derived trend here is for guidance since this data set is not statistically relevant.

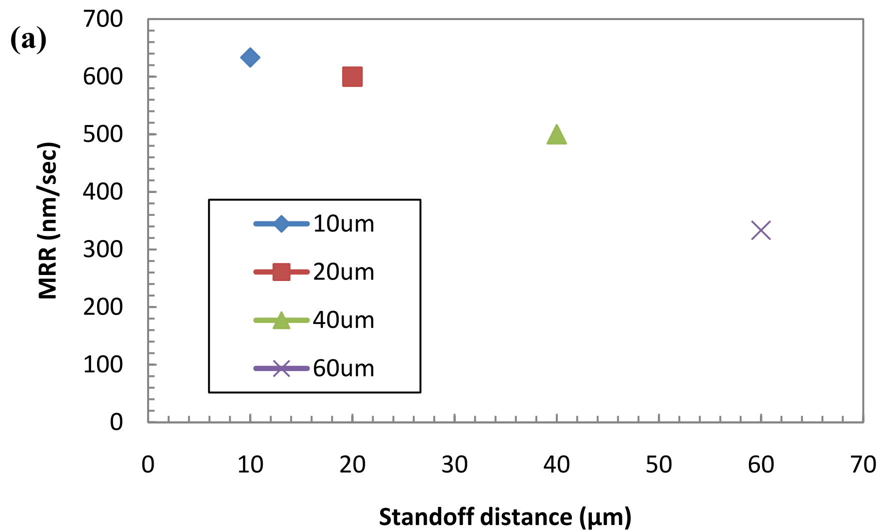

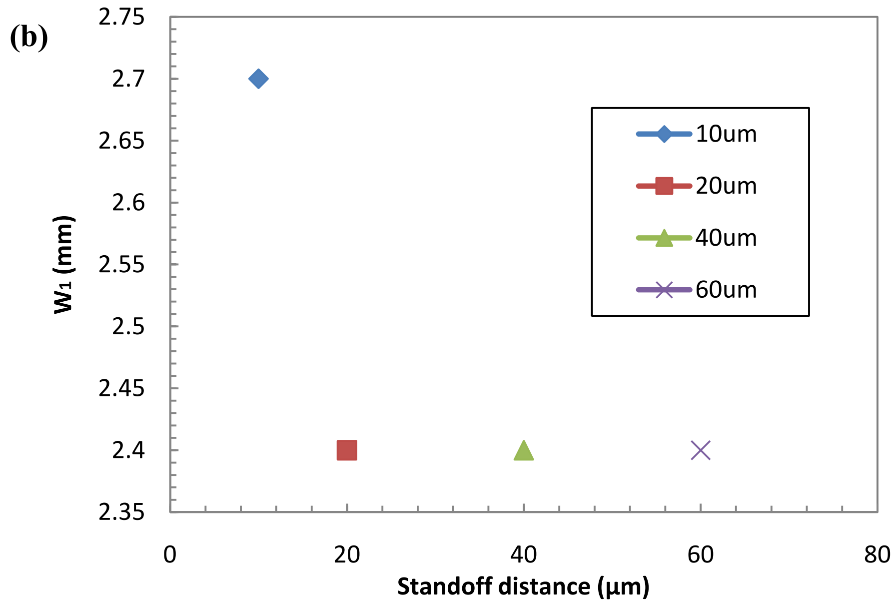

Figure 35 Comparison on (a) material removal rate and (b) printed pattern widths, W_1 at different standoff distance. (CDC voltage, voltage = 3V, pulse duration = 0.5/50msec., exposure = 15sec., electrolyte = 1.80M H_2SO_4 + 0.25M $CuSO_4$)

3.2.4 TEM Mesh with 35µm Window Opening

A large group of experiment has been carried out with the 35µm mesh. Despite the extensive effort and several iterations with DC or CDC voltage control, no satisfactory results were obtained. This section summarizes the results for possible modeling efforts in the future.

3.2.4.1 Roll of applied pressure

TEM mesh 35µm was placed under a polymer sheet with five confining holes of 380µm diameter. This data set is conducted under controlled DC voltage. The objective of applying low suction pressure for TEM mesh 35µm is to prevent bulging happening under the Nafion membrane. Bulging may cause the modulation of electric field being homogeneous and desired pattern will not be printed on copper seed layer. As seen in Figure

36(a) and (b), the profiles of the printed pattern are not sharp at pressure 1.0inHg, even with pressure increase to 1.5inHg. It is suspecting that the emerging electric field after the mask is quite divergent, and thereby greatly diminishing any mask induced modulation. Printed patterns show that MRR is higher at the center and decays towards the edge of the confining hole. The mask pattern is more visible at the edge of the confining hole with large steady erosion and about 10-15% of the total height showing replication of the mask pattern. On Figure 36 (b), the larger blemished region is possibly due to local film delamination.

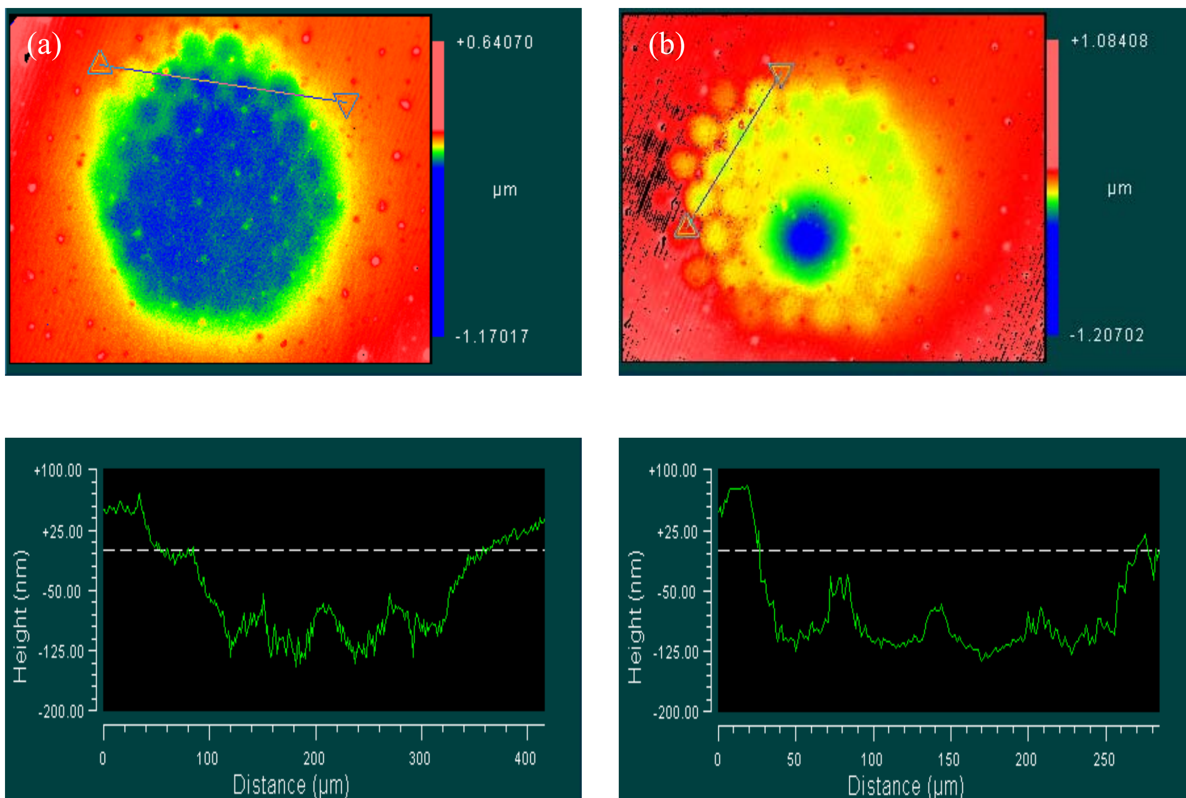

Figure 36 Comparison of different pressure applied for TEM mesh 35µm (not insulated) 2D surface render at 10X. (a) P = 1.0inHg (b) P =1.5 inHg. (DC voltage, applied voltage = 0.1V, standoff distance = 20µm, electrolyte = 0.01M H_2SO_4 + 0.5M $CuSO_4$, exposure = 30sec.)

3.2.4.2 Mesh insulation

The copper TEM mesh is insulated by covering with a thin layer of diluted nail polish and sprayed by air paint brush. The objective of insulating the conductive mesh is to improve its ability to modulate the electric field and transfer the mask pattern. Figure 37 shows mesh patterns were printed by (a) not insulated mesh and (b) insulated mesh, both were conducted under the same experiment settings. The resulting pattern from the insulated mesh (Figure 37(b)) does not show significant improvement as compared to that from un-insulated mesh. The poor quality of the insulated mesh could have been from the inconsistency in the spraying process. Extensive efforts have been devoted to achieve a thin, yet dense layer of the diluted nail polish to coat on the copper TEM mesh. However, the results were not perfect with many clogged pores or uncovered regions.

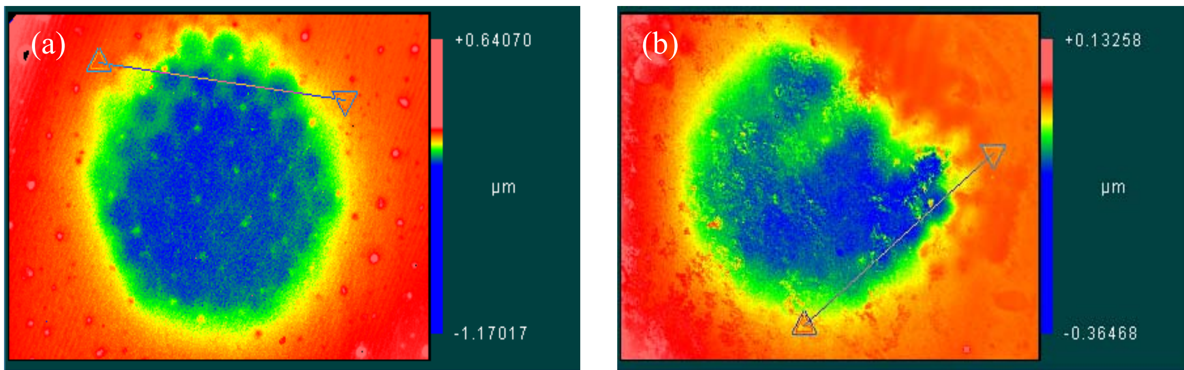

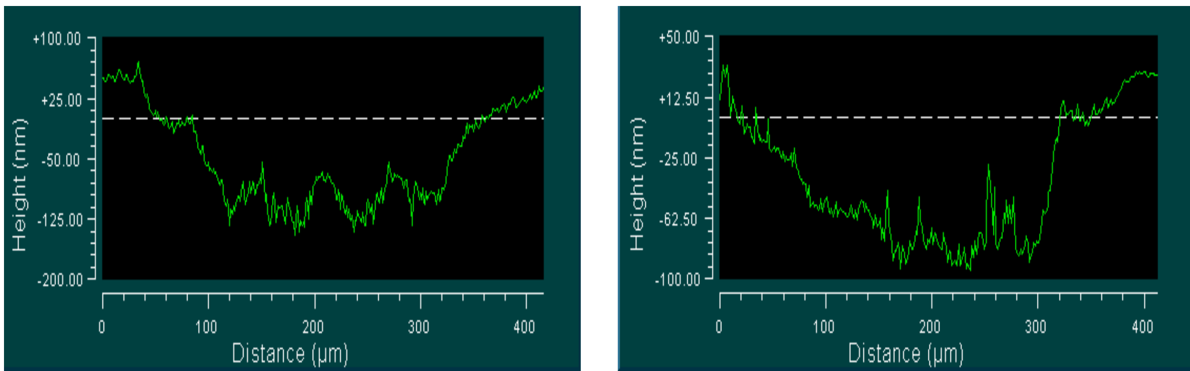

Figure 37 Comparison of insulated and not insulated TEM mesh 35µm 2D surface render at 10X. (a) Mesh not being covered. (b) Mesh covered with thin layer of nail polish and acetone. (DC voltage, applied voltage = 0.1V, standoff distance = 20µm, pressure = 1.0inHg, electrolyte = 0.01M H_2SO_4 + 0.5M $CuSO_4$, exposure = 30sec.)

3.2.4.3 Imprinting under voltage control (CDC)

Several attempts were performed by CDC as a trial to limit the decay of any mask induced modulation to the electric field. The pulse duration was fixed to T_{on} = 0.3µsec., while changing the total pulse period, T_{total} between 30-3000µsec.. The results in Figure 38 show that increasing the relaxation time of the pulse does not show significant improvement of the profile of the printed pattern.

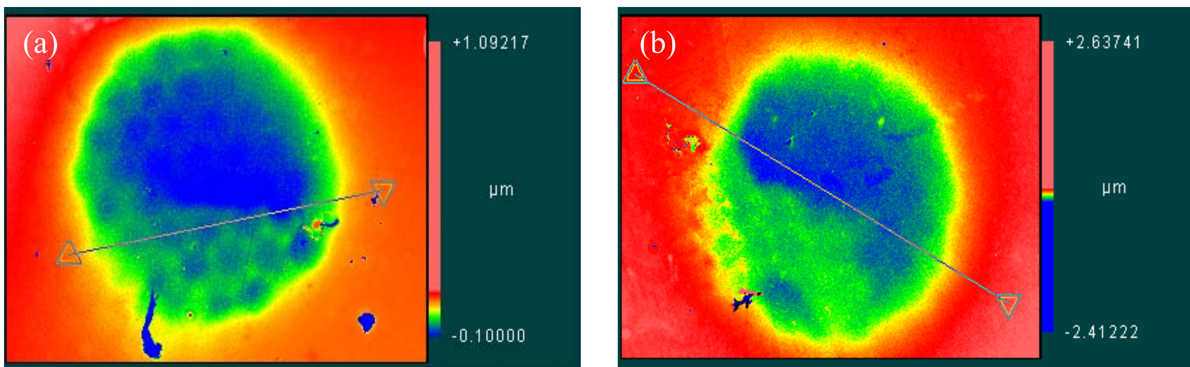

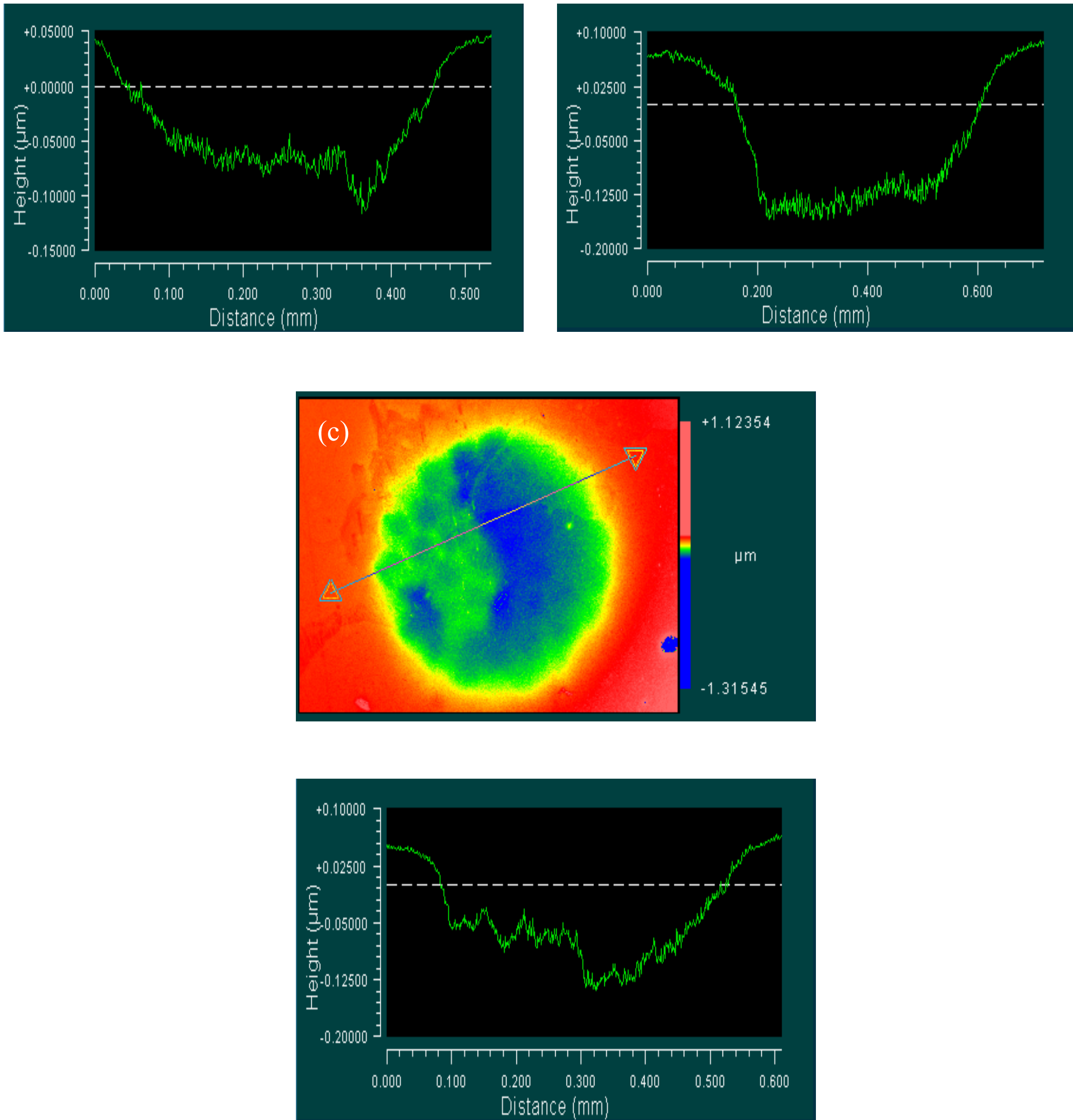

Figure 38 Comparison of increasing total pulse duration (T_{total}) for TEM mesh 35μm 2D surface render at 10X. (a) T_{total} = 30μsec. (b) T_{total} = 300μsec. (c) T_{total} = 3000μsec.. (CDC voltage, applied voltage = 0.5V, standoff distance = 20μm, pressure = 1.0inHg, total pulse duration = 0.3μsec, exposure = 5sec., electrolyte = 0.01M H_2SO_4 + 0.5M $CuSO_4$)

3.3 NON-CONTACT UNIFORM ELECTRIC FIELD MASK PRINTING

3.3.1 TEM mesh with 35µm Window Opening

3.3.1.1 Imprinting under voltage control (DC)

Figure 39 shows that the effect on printed pattern depths and widths while applied voltage increased from 0.1V to 0.5V. The MRR modestly increase with the applied voltage, from 94nm to 108nm. Replicating the original mask is the ultimate goal. The imprinted hole width has a diameter of 20-28% higher than the mask. Figure 40 shows the 2D surface rendering of the printed patterns. In order to improve the imprinted pattern quality, two methodologies have been tried; (i) changing the standoff distance, and (ii) applying CDC voltage control.

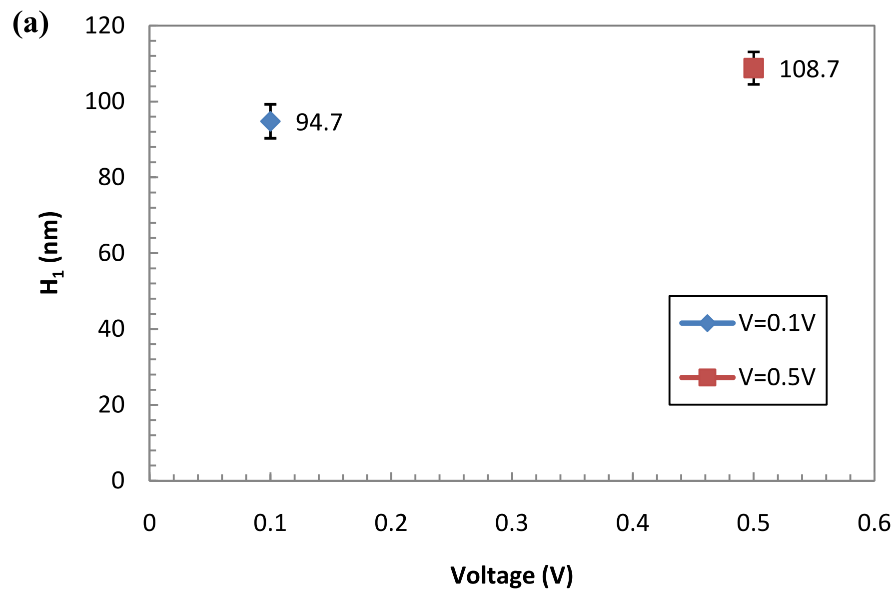

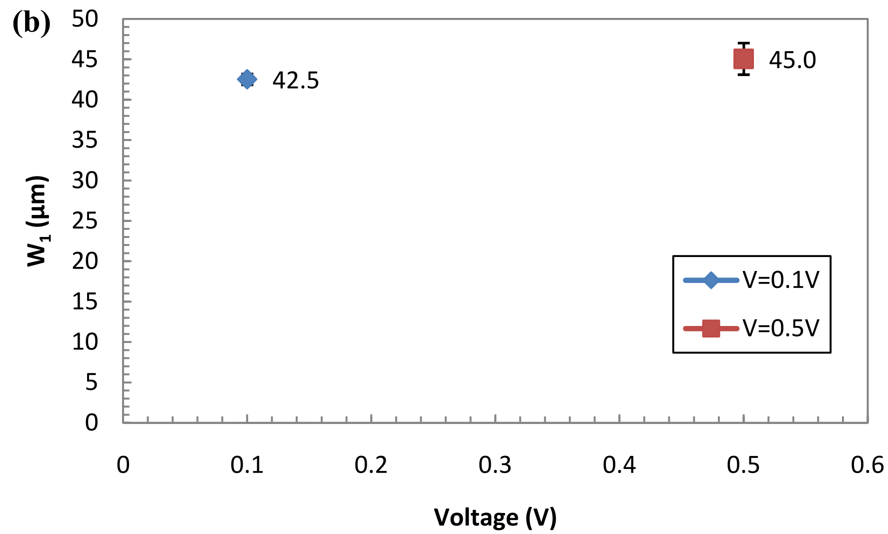

Figure 39 Printed pattern (a) depths, H_1 and (b) widths, W_1 versus applied voltage. (DC voltage, insulated mesh, standoff distance = 20µm, pressure = 1.0inHg, exposure = 30sec., electrolyte = 0.01M H_2SO_4 + 0.5M $CuSO_4$)

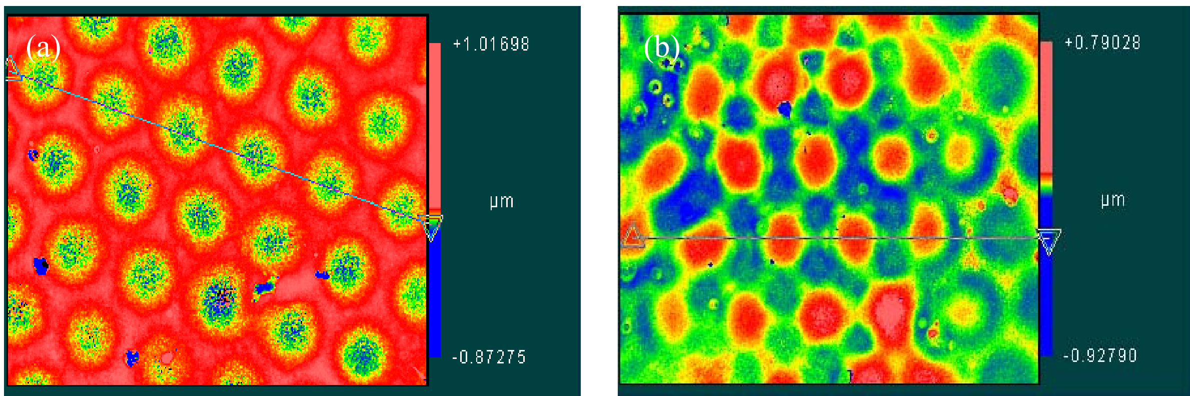

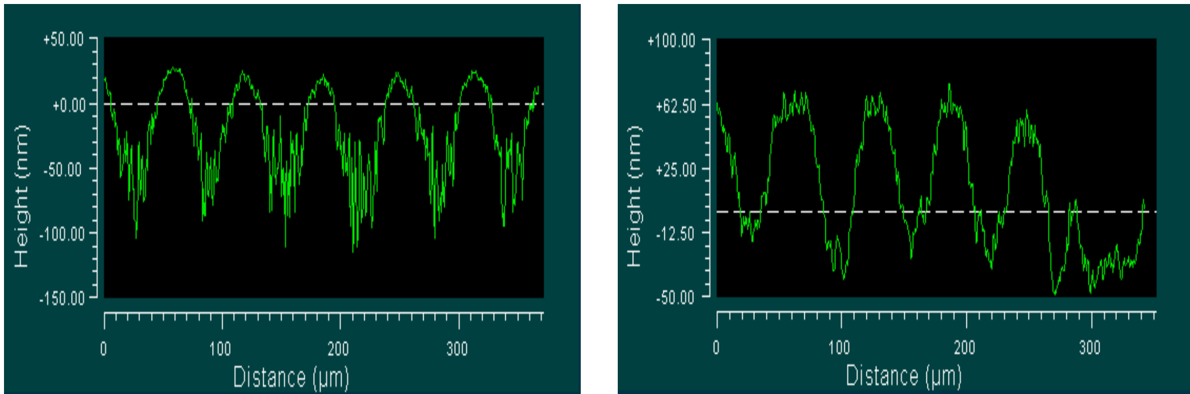

Figure 40 2D surface render on printed 35µm TEM pattern at (a) voltage = 0.1V and (b) voltage = 0.5V. (Mag.=20X) (DC voltage, insulated mesh, standoff distance = 20µm, pressure = 1.0inHg, exposure = 30sec., electrolyte = 0.01M H_2SO_4 + 0.5M $CuSO_4$)

3.3.1.2 Role of standoff distance

Under DC voltage control, the reduction of the standoff distance to 10µm did not show significant enhancement of the imprinted pattern width or on the wall inclination angle as shown in Figure 41. The printed pattern was greater by about 20% from the mask hole dimensions. The wall inclination was less than 1°, and occupies about 25% of the imprinted pattern (Figure 42). The details of the electric field lines with the mask needs further investigation to understand the significant wall erosion of this non-contact mask printing process.

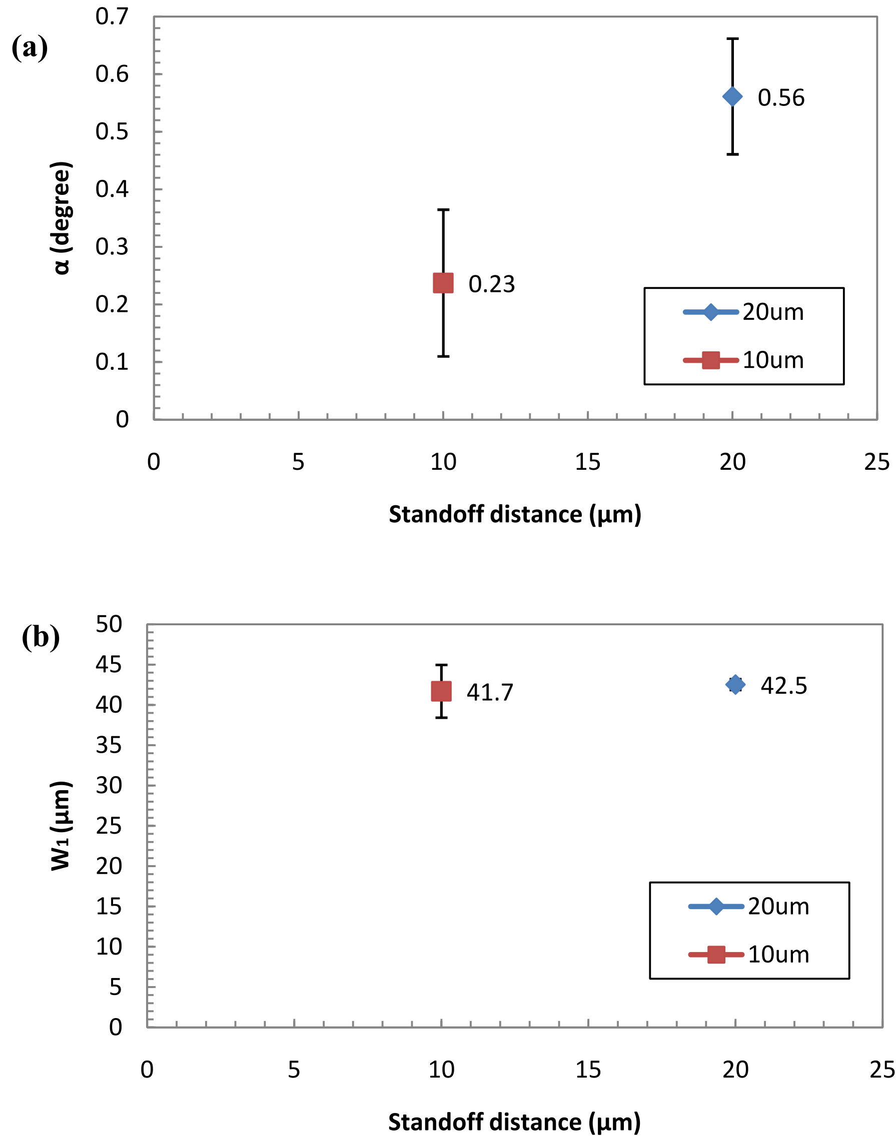

Figure 41 Printed pattern (a) angles, α (b) widths, W_1 versus standoff distance. (DC voltage, insulated mesh, applied voltage = 0.1V, pressure = 1.0inHg, exposure = 30sec., electrolyte = 0.01M H_2SO_4 + 0.5M $CuSO_4$)

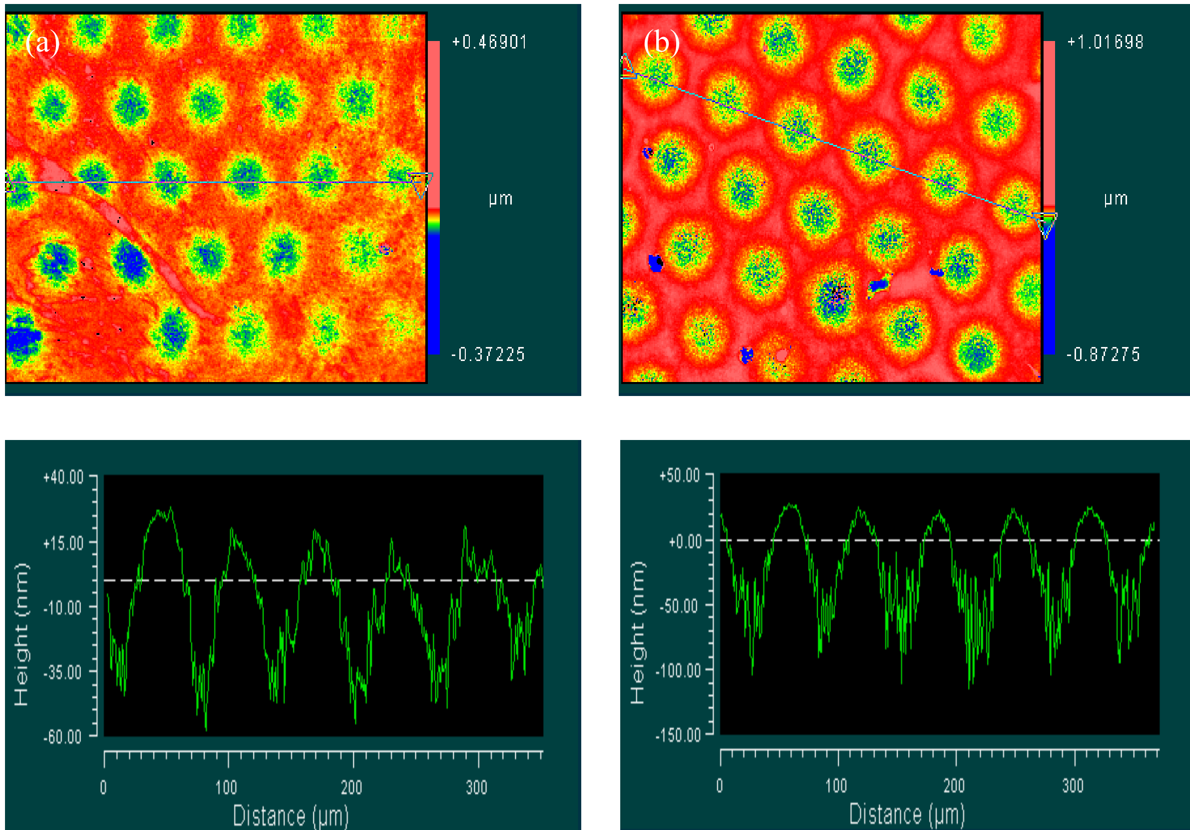

Figure 42 2D surface render on printed 35µm TEM pattern at (a) standoff distance = 10µm and (b) standoff distance = 20µm. (Mag.=20X) (DC voltage, insulated mesh, applied voltage = 0.1V, pressure = 1.0inHg, exposure = 30sec., electrolyte = 0.01M H_2SO_4 + 0.5M $CuSO_4$)

Under CDC voltage control, there was no noticeable improvement of side wall inclination angle. However, instead the width of the imprinted hole was much bigger with a pattern was much worse with 50% increase over the mask hole diameter. Figure 44 shows the 2D surface rendering of the printed patterns. Such data set is counter intuitive; however, it may signify the lateral diffusion effect. Another experimental concern was the conformity of the mask to the workpiece. It is highly likely that an interface standoff distance exists and affected greatly the dissolution process.

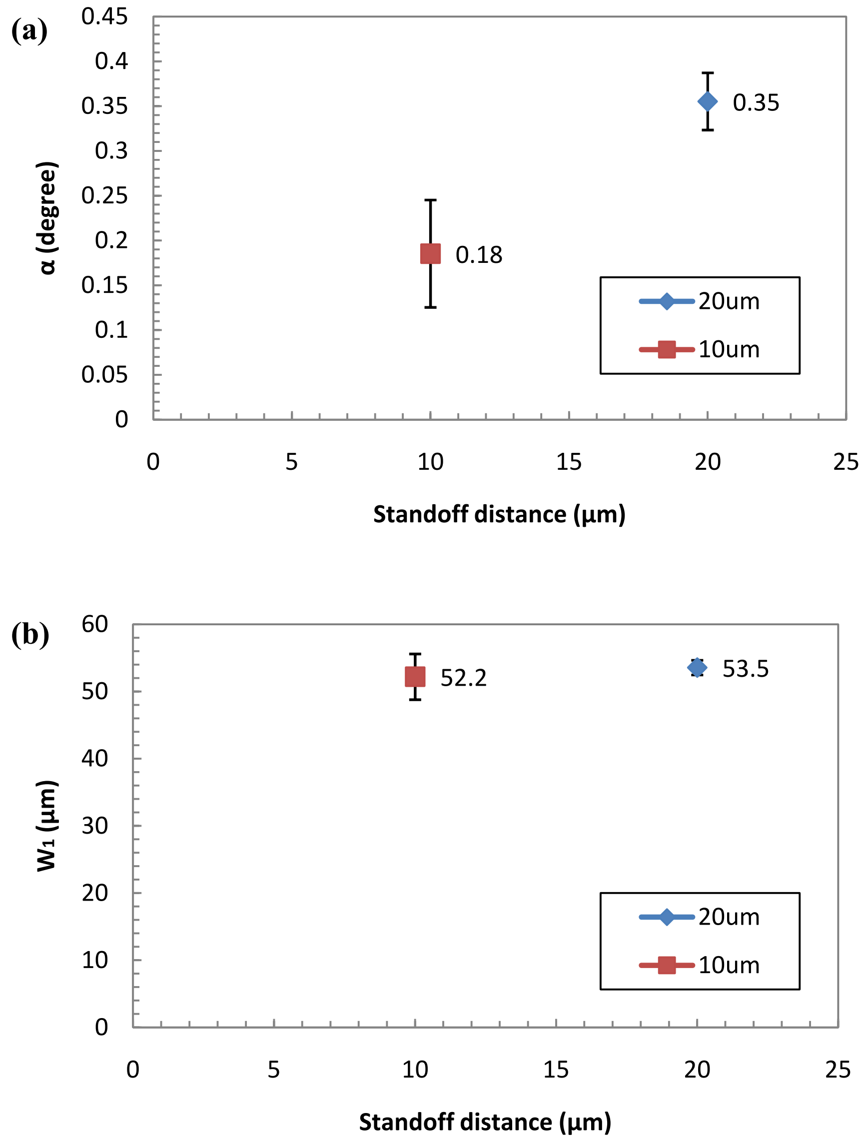

Figure 43 Printed pattern (a) angle, α (b) width, W_1 versus standoff distance. (CDC voltage, insulated mesh, applied voltage = 0.1V, pressure = 1.0inHg, pulse duration = 0.3/30µsec., exposure = 30sec., electrolyte = 0.01M H_2SO_4 + 0.5M $CuSO_4$)

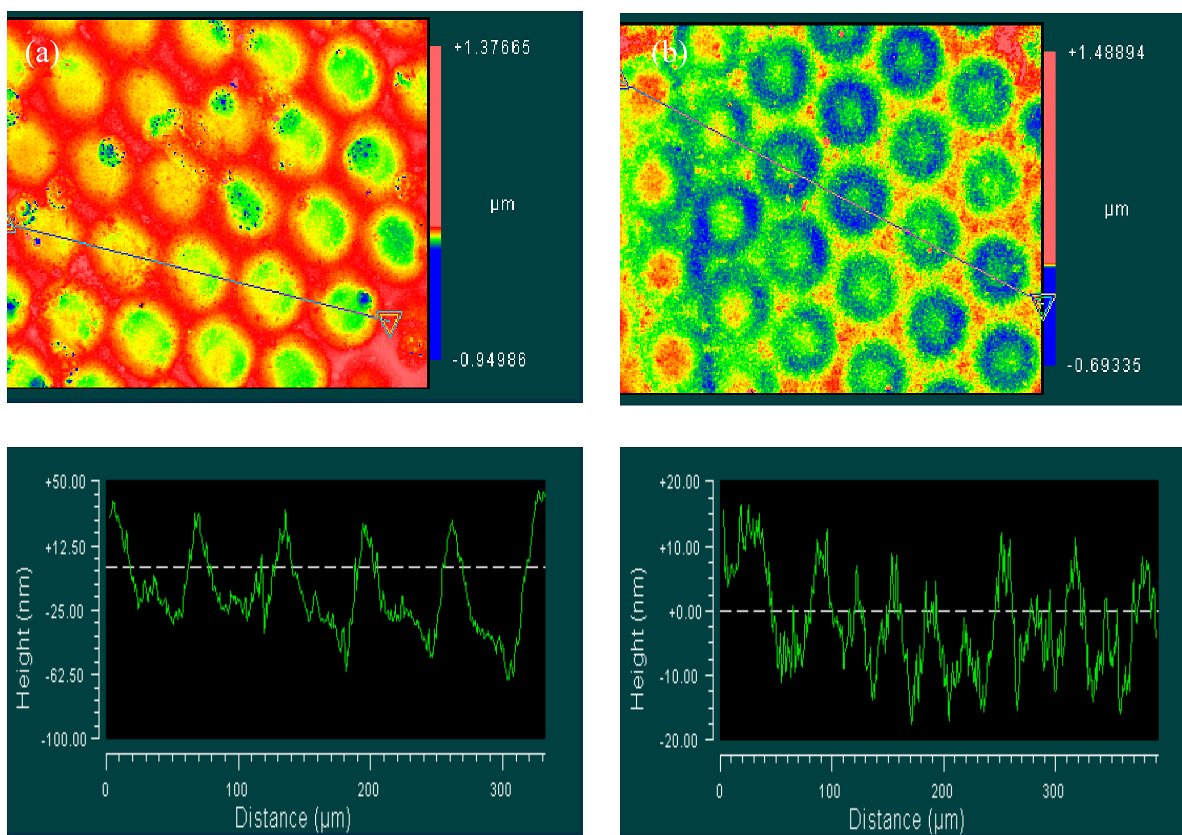

Figure 44 Surface topography and 2D surface render on printed 35µm TEM pattern at (a) standoff distance = 10µm and (b) standoff distance = 20µm. (Mag.=20X) (CDC voltage, insulated mesh, applied voltage = 0.1V, pressure = 1.0inHg, pulse duration = 0.3/30µsec., exposure = 30sec., electrolyte = 0.01M H_2SO_4 + 0.5M $CuSO_4$)

CHAPTER 4: CONCLUSIONS

Micro-manufacturing technology has become an important topic in the fabrication of micro parts and devices. A novel methodology to imprint micron size features on copper surface was successfully adopted in this study via electrochemical machining through selective ion transport membrane. Three different realizations of the mask/membrane assembly were implemented in this study. These realizations are direct contact mask-modulated electric field printing, non-contact mask-modulated electric field printing and non-contact uniform electric field mask printing.

Direct contact mask-modulated electric field printing method has shown the best overall printing accuracy among two other printing methods. In this method a replica of the mask ligaments is produced. Best results were obtained for pulse duration at the 500MHz range and pulse period of 50kHz. The imprinted trench width is about 40 to 60% of the mask dimensions. This indicates feature shrinking. The trench walls have an angle of about 20°, about two order of magnitude above the other two methods. There was a wider entrance at the top of the trench of about twice the mask ligament size. These observations and estimates are based on the entire width of the mask ligament. However the mask ligament may have edge details of the same order of the imprinted pattern. Thus, the reported reduction should be requalified based on the actual mask edge morphology. The experimental measurements showed that there is a threshold voltage, below which no material removal would occur. The MRR then becomes nearly liner with the applied voltage for the range of measurements conducted in this study.

Modulated electric field printing method has shown very limited success with mask replication, especially with features generally less than 35µm (based on the examined range of dimensions). The mask role in this method is to modulate the applied electric field via blocking the field lines. This process takes place after building up counter charges on the non-conductive zones of the mask. It seems that the charge build up in this configuration was highly unstable with continuous charge leakage into the bulk of the electrolyte. Thus, any imposed modulation from the mask has been significantly decayed. The imprinted pattern has a large amount of uniform erosion with about 10-15% of its total height showing replication of the mask features. The utilization of CDC at MHz frequency did not provide much improvement. It seems that charge build up time constant is much longer than these high frequency applied electric field. For larger features in the range of 100µm or more, better replication results of the mask opening were obtained with good overall profile. The MRR showed strong dependence on the location of the cathode electrode from the mask. However the pattern profile was insensitive to the electrode location. The MRR was inversely proportional to the standoff distance from the workpiece. The MRR showed also a strong dependence on the electrolyte concentration and conductivity in the range of (30 to 50 mS/cm). Beyond this range, the MRR showed limited improvement. The suction pressure induced membrane curvature has shown some promises for the possibility of focusing or modulating the electric field.

The non-contact uniform electric field mask printing method has shown some promises in replicating the opening of a mask that is in direct contact with the imprinted surface. However, the imprinted profile was about 20% larger than the mask opening. CDC

did not show much improvement when utilized, but rather provided 50% larger openings than the mask. These larger opening may not be conclusive evidence that the direct contact of the mask and imprinted surface would result in a wider pattern. Instead, it is possible the continuous erosion from charge build has taken place simultaneously. Additional measurements are needed to understand the macro topology of the imprinted pattern.

To conclude, the developed printing process via electric field induced ion transport across cation selective membrane showed reasonable success within the three realizations discussed here. Elaborated modeling of the details of the temporal electric field evolution and charge accumulation at the cathode chamber film interface and at the workpiece electrolyte interface may shed more lights on the details of the process.

CHAPTER 5: FUTURE WORK

The current study has shown the ability of the FEFIIT process to successfully imprint micron size features. The focus of current study was to experimentally explore the design space parameters and their role on the quality of the imprinted patterns. Once these correlations are established, detailed modeling is needed to understand the limits of the transport phenomena at the workpiece electrolyte interface and at the Nafion® membrane cathode interface. The spatial variation and modulation of the electric field is of utmost importance in defining the details of the imprinted profile. The details of the measurements presented in this thesis would act as the foundational for developing and calibrating such modeling framework.

Perfecting current experiment apparatus is considered as part of the future work to achieve outstanding experimental results. A motorized XYZ stage equipped with displacement sensor is mandatory to accurately measure the separation distance between cathode chamber and work piece. In order to prevent leakage of the electricity from the cathode chamber to the system, designing a polymer made cathode chamber and specifying the electrode location will be needed.

REFERENCES

1. Rajurkar K. P., Levy G., Malshe A., Sundaram M. M., McGeough J., Hu X., Resnick R., DeSilva A., *Micro and nano machining by electro-physical and chemical processes*.

2. Brown T. L., LeMay H. E. and Bursten B. E., (April 2000) *Chemistry The Central Science*, Prentice Hall, Upper Saddle River, N. J., Eighth Edition.

3. Bard A.J., Faulkner L.R., (2001) *Electrochemical Methods: Fundamentals and Applications*, John Wiley & Sons Inc., 605 Third Avenue, N. Y., Second Edition.

4. Huo J., Solanki R., McAndrew J., (2004) *Study of anodic layers and their effects on electropolishing of bulk and electroplated films on copper*, Journal of Applied Electrochemistry, Vol 34: 305-314.

5. Jonassen N., (1998) *Electrostatics*, Chapman & Hall, New York.

6. Hockey S.W., (1972) *Fundamental Electrostatics*, Methuen Education Ltd., Fakenham, Norfolk.

7. Brask A., (February 2003) *Principles of Electroosmotic Pumps*, Technical University of Denmark.

8. Husser O. E., Craston D. H., Bard A. J., (1989) *Scanning Electrochemical Microscopy High-Resolution Depositionand Etching of Metals*, Journal of The Electrochemical Society, Vol. 136, No. 11.

9. Craston D. H., Lin C. W., Bard A. J., (1988) *High Resolution Deposition of Silver in Nafion Films with the Scanning Tunneling Microscope*, Journals of The Electrochemistry Society, 785, 786.

10. Schuster R., Kirchner V., Allongue P., Ertl G., (2000) *Electrochemical micromachining*, Science, Vol. 289.

11. Kock M., Kirchner V., Schuster R., (2002) *Electrochemical micromachining with ultrashort voltage pulses – a versatile method with lithographical precision*, Electrochimica Acta 48 3213-3219.

12. Kirchner V., Cagnon L., Schuster R., Ertl G., (2001) *Electrochemical machining of stainless steel microelements with ultrashort voltage pulses*, Applied Physics Letters, Volume 79, Number 11.

13. Lee E. S., Baek S. Y., Cho C. R., (2007) *A study of the characteristics for electrochemical micromachining with ultrashort voltage pulses*, International Journal of Advance Manufacturing Technology, Vol. 31, 762-769.

14. Kim B. H., Ryu S. H., Choi D. K., Chu C. N., (2005) *Micro electrochemical milling*, Journal of micromechanics and microengineering, Vol. 15, 124-129.

15. Mazur S., Foggin G. W., Jackson C. E., Chase B., (2008) *Membrane-Mediated Electropolishing of Copper*, Journal of The Electrochemical Society, 155 (4) H235-H242.

16. Zawodzinski T. A., Springer T. E., Davey J., Jestel R., Lopez C., Valerio J., Gottesfeld S., (July 1993) *A Comparative study of water uptake by and transport through ionomeric fuel cell membranes*, Journal of The Electrochemical Society, Vol. 140, No. 7.

17. Solasi R., Zou Y., Huang X., Reifsnider K., (2007) *A time and hydration dependent viscoplastic model for polyelectrolyte membranes in fuel cells*, Mech Time-Depend Mater 12: 12-30.

ACKNOWLEDGEMENT

First of all, I would like to express my deepest sense of gratitude to my advisor, Dr. Ashraf Bastawros for his encouragement and excellent guidance throughout the entire research. Despite his busy schedules, he is always there for students, offering support, discussing new ideas and making sure students are walking on the correct path. I owe Dr. Bastawros more than I can say for his persistence, patience, insight and support.

A special thanks to my very good friend, Shakti S. Chauhan (soon to be Dr. Chauhan) for his support and helpful discussions. I am thankful to all the members of Micro-nano Mechanics Research Group for their support and it is an enjoyable experience working with them as a team.

Last but not least, I would like to thank my girl friend, Amy Chen, who has been giving me support and encouragement every day and believe in me. I take this opportunity to express my profound gratitude to my beloved parent, Ka-Aik Low and Bee-Kuen Lai.

This research is supported by National Science Foundation Grants NSF-CMMI-0654162 and NSF-CMMI- 0700045.